

## Original Article

**Cite this article:** Calvès G, Mix A, Giosan L, Clift PD, Brusset S, Baby P, and Vega M (2022) The Nazca Drift System – palaeoceanographic significance of a giant sleeping on the SE Pacific Ocean floor. *Geological Magazine* **159**: 322–336. <https://doi.org/10.1017/S0016756821000960>

Received: 21 November 2019

Revised: 19 July 2021

Accepted: 26 August 2021








First published online: 2 November 2021

**Keywords:**

Nazca Ridge; Nazca Drift System; Contourite drift; Oligocene; SE Pacific Ocean; palaeoceanography

**Author for correspondence:** Gérôme Calvès, Email: [gerome.calves@univ-tlse3.fr](mailto:gerome.calves@univ-tlse3.fr)

# The Nazca Drift System – palaeoceanographic significance of a giant sleeping on the SE Pacific Ocean floor

Gérôme Calvès<sup>1</sup> , Alan Mix<sup>2</sup> , Liviu Giosan<sup>3</sup> , Peter D. Clift<sup>4</sup> , Stéphane Brusset<sup>1</sup> , Patrice Baby<sup>5</sup>  and Mayssa Vega<sup>6</sup> 

<sup>1</sup>Université Toulouse III, GET-OMP, 14 avenue Edouard Belin, 31400, Toulouse, France; <sup>2</sup>College of Earth, Ocean, and Atmospheric Sciences, Oregon State University, Corvallis, OR 97331, USA; <sup>3</sup>Geology & Geophysics, Woods Hole Oceanographic Institution, Woods Hole, MA 02543, USA; <sup>4</sup>Department of Geology and Geophysics, E235 Howe-Russell, Louisiana State University, Baton Rouge, Louisiana 70803, USA; <sup>5</sup>IRD, GET-OMP, 14 avenue Edouard Belin, 31400, Toulouse, France and <sup>6</sup>Universidad San Antonio Abad del Cusco, Av. De la Cultura 773, 08000 Cusco. Peru

**Abstract**

The evolution and resulting morphology of a contourite drift system in the SE Pacific oceanic basin is investigated in detail using seismic imaging and an age-calibrated borehole section. The Nazca Drift System covers an area of 204 500 km<sup>2</sup> and stands above the abyssal basins of Peru and Chile. The drift is spread along the Nazca Ridge in water depths between 2090 and 5330 m. The Nazca Drift System was drilled at Ocean Drilling Program Site 1237. This deep-water drift overlies faulted oceanic crust and onlaps associated volcanic highs. Its thickness ranges from 104 to 375 m. The seismic sheet facies observed are associated with bottom current processes. The main lithologies are pelagic carbonates reflecting the distal position relative to South America and water depth above the carbonate compensation depth during Oligocene time. The Nazca Drift System developed under the influence of bottom currents sourced from the Circumpolar Deep Water and Pacific Central Water, and is the largest yet identified abyssal drift system of the Pacific Ocean, ranking third in all abyssal contourite drift systems globally. Subduction since late Miocene time and the excess of sediments and water associated with the Nazca Drift System may have contributed to the Andean orogeny and associated metallogenesis. The Nazca Drift System records the evolution in interactions between deep-sea currents and the eastward motion of the Nazca Plate through erosive surfaces and sediment remobilization.

**1. Introduction**

The Nazca Ridge separates the Chile and Peru oceanic basins (Fig. 1a) (e.g. Kukowski *et al.* 2008), which have their shallowest closed bathymetric contour at 3600 m water depth. These basins are open at sills and trenches where bottom water flow connects to the surrounding basins (Lonsdale, 1976; Harris *et al.* 2014; Harris & Macmillan-Lawler, 2018). The Nazca Ridge is a bathymetric high marked by numerous seamounts with an elongated and rough morphology (Harris *et al.* 2014; Casalbore, 2018). This aseismic ridge is being subducted under the South American Plate (Pilger, 1981) where it is interacting with the active margin by increasing tectonic erosion (von Huene *et al.* 1996; Hampel, 2002; Clift *et al.* 2003; Hampel *et al.* 2004). Its influence is felt as far inboard as the Andes (e.g. Gutscher *et al.* 1999; Rousse *et al.* 2003) and possibly the Amazon foreland basin (Espurt *et al.* 2007). Two Ocean Drilling Program (ODP) sites, 1236 and 1237, have drilled this ridge, coring Oligocene to Recent sediments with pelagic to hemipelagic facies (Tiedemann & Mix, 2007; Fig. 1a).

This region of the SE Pacific Ocean is a key location for understanding the interplay between plate tectonics and climate change, because the oceanic domain is under the influence of southern and equatorial atmospheric cells and is famous for the Humboldt Current that flows along the coast of South America (von Humboldt, 1816; Shaffer *et al.* 2004; Chaigneau *et al.* 2013). In this region the moving water masses are the intermediate water of the Pacific Central Water (PCW; 1500–3000 m), which has a southward movement, and the deep waters of the Circumpolar Deep Water (CDW, also known as CPDW; >3000 m) that flows northward (Fig. 1b, c; Emery & Meincke, 1986; Tsuchiya & Talley, 1998; Talley, 2013; Emery, 2019). The shallow-water currents are the Peru Coastal Current (PCC) and the Peru Oceanic Current (POC) (Fig. 1a). The active deep-water currents are the poleward Peru–Chile Undercurrent (PCUC) and Peru–Chile Counter Current (PCCC), as well as the northward flowing Chile–Peru Deep Coastal Current (CPDCC; Chaigneau *et al.* 2013). The flow of water from the Sub-Antarctic Mode Water/Antarctic Intermediate Water (SAMW/AAIW) into the Chile Basin is characterized by a total equatorward transport of *c.* 7 Sv (Shaffer *et al.* 2004). The bottom

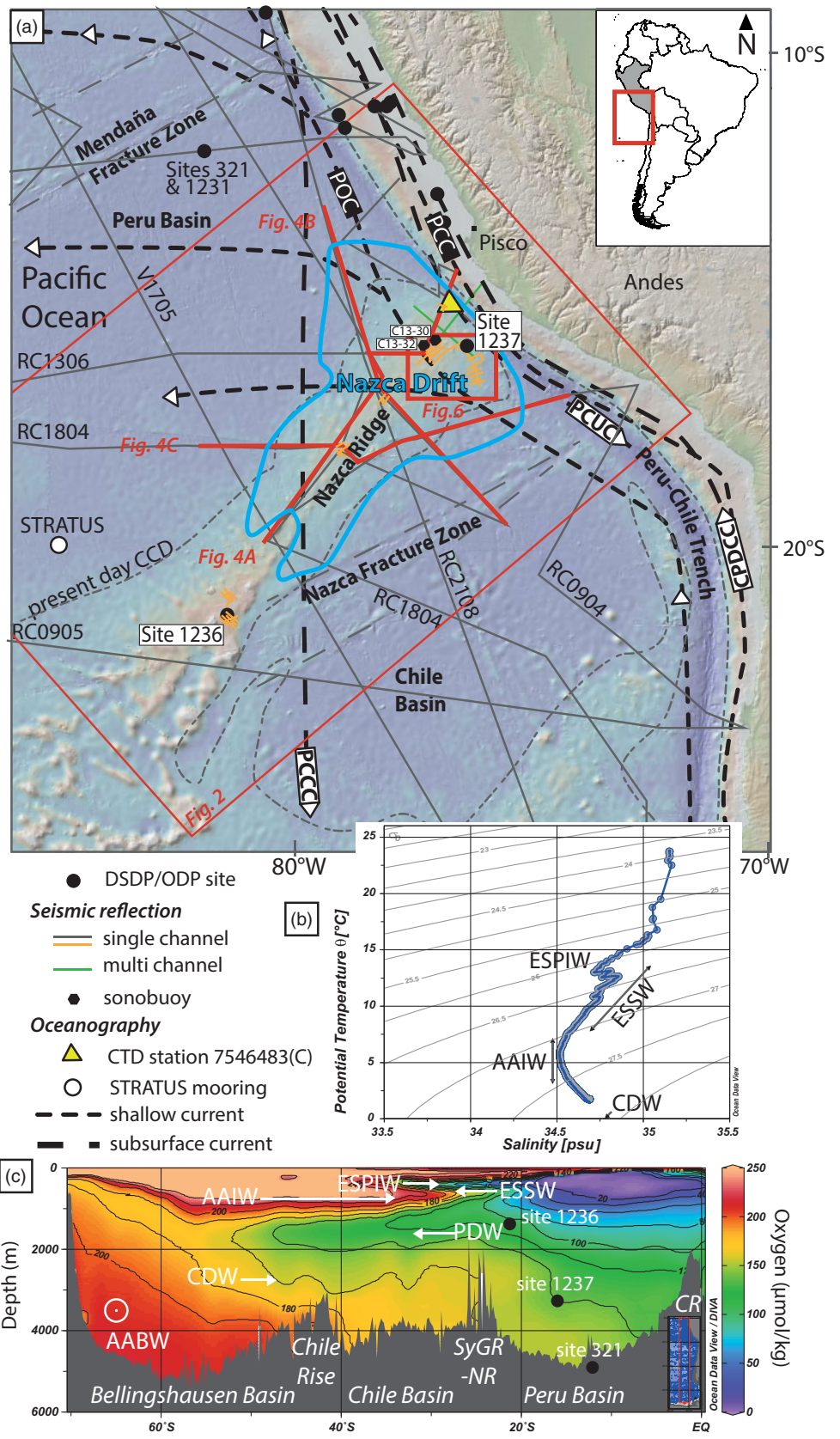


**Fig. 1.** (Colour online) (a) Bathymetry and topography of the SE Pacific locating the Nazca Drift System with a blue outline (black lines; data from: single channel seismic lines from Marine Geoscience Data System, <https://www.marine-geo.org>; R/V Sonne cruise SO146-GEOPECO (green lines; Hampel *et al.* 2004) and GENE03RR (orange lines; Mix, 1997). Sonobuoy data C13-30 and C13-32 are located near ODP Site 1237 (J. B. Diebold, unpub. data table, 1996: sediment and crustal velocities from sonobuoy solutions; accessed from <http://www.geomapapp.org>, 2019). Arrows indicate general flow directions of surface currents (black short dots bold line; PCC – Peru Coastal Current; POC – Peru Oceanic Current) and subsurface currents (black long dots bold line; PCCC – Peru-Chile Countercurrent; CPDCC – Chile-Peru Deep Coastal Current; PCUC – Peru-Chile Undercurrent) (e.g. Chaigneau *et al.* 2013) along the Peru-Chile margin. Drilling sites are from DSDP and ODP Legs 112, 138 and 202 (Shipboard Scientific Party, 1988, 1992, 2003a). STRATUS mooring is located west of the study area (<https://www.pmel.noaa.gov/co2/story/Stratus>). (b) Temperature-salinity diagram at CTD station 7546483(C) (yellow triangle in (a); 15.373°S; 76.751°W). (c) Hydrographic section of the SE Pacific sector, oxygen concentrations showing major water masses and boundaries. AABW – Antarctic Bottom Water; AAIW – Antarctic Intermediate Water; CDW – Circumpolar Deep Water; ESPIW – South Pacific Intermediate Water; ESSW – Equatorial Subsurface Water; PDW – Pacific Deep Water. Ridges: SyGR – Sala y Gomes Ridge; NR – Nazca Ridge; CR – Carnegie Ridge.

waters within the study area are dominated by the AAIW and the CDW (Fig. 1b). Oxygen concentrations along a hydrographic section from the Southern Ocean to the equator (c. 85° W) illustrate

the vertical and spatial organization of the water masses and the direction of the current flow (Fig. 1c). In the SE Pacific Ocean, the deeper water masses consist of 40–60 % Antarctic Bottom

Water (AABW) and 20–30% North Atlantic Deep Water (NADW), but it is important to note that the CDW was not included in this analysis (Johnson, 2008). The CDW is the bottom water now active in the SE Pacific north of the Chile Rise and is not affected by the AABW (Tsuchiya & Talley, 1998; Talley, 2013). The Peruvian margin is strongly eroded by the bottom currents from the shelf to the base of slope (Calvès *et al.* 2017). The influence of the Andes and its uplift on oceanic currents has been modelled (Sepulchre *et al.* 2009) despite limited documentation of geological features (Lonsdale & Malfait, 1974; Lonsdale, 1976) related to oceanic currents, such as the Humboldt Current. The SE Pacific is under the influence of the Antarctic Circumpolar Current (ACC), with a dated onset during Oligocene time (e.g. Barker *et al.* 2007; Lyle *et al.* 2007; Scher *et al.* 2015). This setting of oceanic basins and bathymetric highs bathed by moving water masses is prone to erosion and transport of sediments by bottom water current action and thus the emplacement of contourite drifts (Lonsdale & Malfait, 1974; Lonsdale, 1976; Esentia *et al.* 2018; Juan *et al.* 2018), despite low predicted velocities at the seafloor (Thran *et al.* 2018). We document the first regional compilation of surface and subsurface data to describe the Nazca Drift System in the evolution of the southern hemisphere oceanic cell. More generally we seek to understand the role that the vertical motion of water masses and seafloor bathymetry has had in shaping open ocean contourite drifts in the SE Pacific Ocean since Oligocene time.

## 2. Methods

Data are sourced from various vintage seafloor bathymetric surveys and seismic reflection acquisitions acquired since the 1960s (NOAA-NCEI; <https://www.ngdc.noaa.gov/mgg/mggd.html>). The main source of regional seismic profiles is the analogue seismic reflection profile databank at the Lamont-Doherty Earth Observatory (LDEO) and single channel seismic (SCS) profiles RC0904, RC0905, RC1306, RC1307, RC1804 and RC2108 (<https://www.ngdc.noaa.gov/mgg/seismicreflection/index.html>). A more recent seismic reflection site survey (GENEO3RR, 1997) was acquired to plan drilling sites for ODP Leg 202 (Fig. 1a; Tiedemann & Mix, 2007). The vintage SCS have a lower vertical resolution compared to the modern SCS, which have a peak frequency of 55–60 Hz. ODP Site 1237 provides ages for calibrating the seven interpreted seismic reflections from the acoustic basement to the seafloor (Tiedemann & Mix, 2007).

The seafloor has been mapped using multibeam bathymetric data (NOAA-NCEI multibeam bathymetry; <https://www.ngdc.noaa.gov/maps/autogrid/>) across the Nazca Ridge and surrounding Peru and Chile basins (Fig. 2a). The regional bathymetry is sourced from the General Bathymetric Chart of the Oceans (GEBCO) Compilation Group (2019; [https://www.gebco.net/data\\_and\\_products/gridded\\_bathymetry\\_data/](https://www.gebco.net/data_and_products/gridded_bathymetry_data/)). The main lithologies cropping out at the seafloor are calcareous oozes and other fine-grained calcareous sediments overlying the Nazca Ridge igneous basement, and siliciclastic clay and diatom oozes in the surrounding basins (Dutkiewicz *et al.* 2015; [https://www.earthbyte.org/webdav/ftp/papers/Dutkiewicz\\_et\\_al\\_seafloor\\_lithology/](https://www.earthbyte.org/webdav/ftp/papers/Dutkiewicz_et_al_seafloor_lithology/)). In this study we follow the seafloor geomorphologic analysis of Harris *et al.* (2014) (Fig. 2b). The seismic dataset spanning the Nazca Ridge and surrounding area covers most of the different abyssal to trench settings (or features) identified by Harris *et al.* (2014). Seafloor depths range from 1550 to 5270 m in the SE Pacific Ocean, offshore Peru (Fig. 1a). The uninterpreted seismic

data are provided in the online Supplementary Material Figures S1 and S2. The seismic data displayed in this study are zero phase and have the Society of Exploration Geophysicists normal polarity, i.e. black peak indicating an increase in acoustic impedance. With a dominant frequency of 55–60 Hz and a velocity of 1800 m s<sup>-1</sup>, the seismic resolution, defined as a quarter of the dominant wavelength, would be 7–9 m. We use a constant velocity (1500 m s<sup>-1</sup>) for depth conversion of the seafloor from time to depth domain. Depth conversions of the sediments are based on a velocity of 1800 ± 200 m s<sup>-1</sup> derived from the refraction profiles in the eastern part of the study area (Hampel *et al.* 2004) and two sonobuoy solutions (C13-30 and C13-32; Fig. 1; J. B. Diebold, unpub. data table, 1996: sediment and crustal velocities from sonobuoy solutions; accessed from <http://www.geomapapp.org>, 2019). No velocity measurements on sediments or wireline logs have been acquired within the study area.

The 2-D seismic data in this study have been interpreted using standard seismic stratigraphic techniques (Mitchum *et al.* 1977; Vail *et al.* 1977) based on reflection terminations and seismic facies reflection characteristics (amplitude, frequency). The seafloor reflection shows concordance (no termination) or truncation (erosional or structural) and together with the surrounding reflections is interpreted as a sequence boundary (Mitchum *et al.* 1977). A megasequence is defined as being between the acoustic basement and the seafloor reflection. In the focus study area near ODP Site 1237, a detailed analysis of the seismic units with age calibration is possible (Fig. 1). The seismic facies identified are summarized in Figure 3. Two classes of seismic facies are observed, the first is associated with volcanic/oceanic crust features (e.g. Calvès *et al.* 2011) and the second with bottom current-induced sedimentary features (e.g. Faugères *et al.* 1999; Rebesco & Stow, 2001; Hernández-Molina *et al.* 2008; Dubois & Mitchell, 2012; Rebesco *et al.* 2014 and references therein; Stow *et al.* 2019; Bailey *et al.* 2021). A regional cross-section and isopach map of the entire megasequence allows identification of the main depocentres (Fig. 4). Oceanographic data (temperature, salinity, oxygen) are sourced from the National Oceanic and Atmospheric Administration (NOAA) World Ocean Database (WOD13) (Boyer *et al.* 2013).

## 3. Results

### 3.a. Seafloor morphology

The Nazca Ridge divides the study area along a SW–NE axis and separates the Chile and Peru basins (Fig. 2a). Within the study area we have identified, seaward of the Peru–Chile Trench, the transition of seafloor types/morphologies from faulted oceanic crust type morphology ( $\alpha$ , Fig. 2a), volcanic mound/seamount ( $\beta$ , Fig. 2a), to smooth seafloor associated with hemipelagic sedimentation and contourite drifts ( $\gamma$ , Fig. 2a). The faulted oceanic crust seafloor type shows various sedimentary covers, with a very thin drape towards the spreading centre of the East Pacific Rise to a thicker sedimentary cover and smoother seafloor towards the trench. The oceanic crust around the Nazca Ridge is linked to fast seafloor spreading at c. 100 mm yr<sup>-1</sup> (Wright *et al.* 2016), as expressed by the numerous faults observed at the seafloor (Fig. 2a, inset  $\alpha$ ) that mark the abyssal hills and abyssal plains (Cormier & Sloan, 2018). Near the trench, the oceanic crust and overlying sediments are affected by normal faults caused by the bending of the plate by subduction (Kukowski *et al.* 2008). This bending extends c. 150 km from the trench axis and progressively advances as the Nazca Ridge is subducted, but this only affects a rather small part of the area

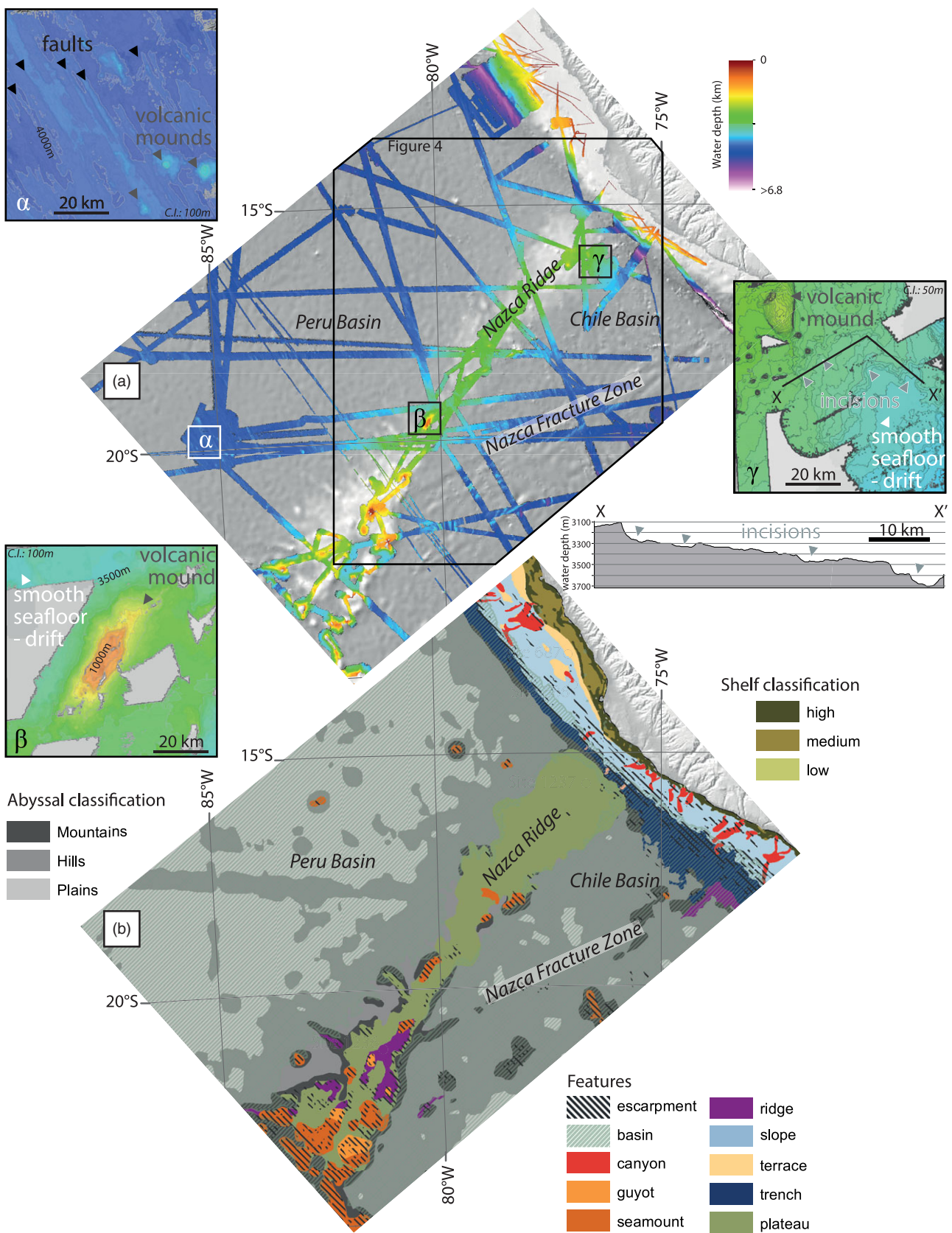
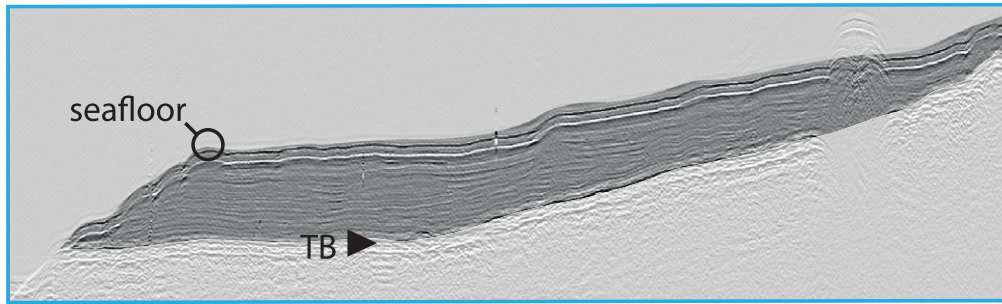
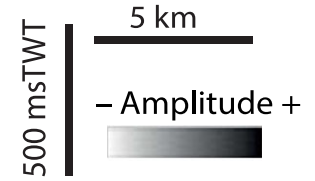


**Fig. 2.** (Colour online) Seafloor bathymetry and geomorphology of the Nazca Drift System and the surrounding basins. (a) Multibeam (in colour, NOAA-NCEI; <https://www.ngdc.noaa.gov/maps/autogrid/>) and GEBCO (greyscale; [https://www.gebco.net/data\\_and\\_products/gridded\\_bathymetry\\_data/](https://www.gebco.net/data_and_products/gridded_bathymetry_data/)) bathymetry of the study area. Insets: examples of three different seafloor geomorphologies: ( $\alpha$ ) faulted oceanic crust, ( $\beta$ ) volcanic seamount, and ( $\gamma$ ) smooth seafloor/drift (CI – contour interval). (b) Seafloor typology from interpretation of Harris *et al.* (2014).

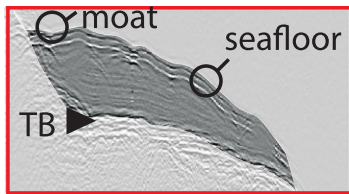
(a) **Plastered drift**



Length: 10-25 km  
Height: 10-280 msTWT

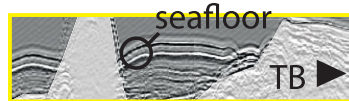


(b) **Mounded separated/isolated drift**



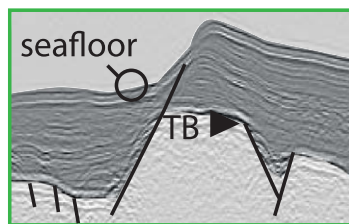
Mound / low amplitude  
Moat on the edge of high  
Background: parallel to wavy  
Height: 0-250 msTWT  
Length: 5-10 km

(c) **Confined drift**



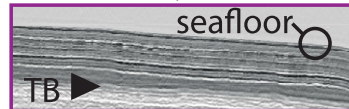
Mound / low to high amplitude  
Moat on the edges of highs  
Background: parallel to wavy  
Length: 10->100s km  
Height: 10-100 msTWT

(d) **Fault/scarp controlled drift**



Mound-wedge / low amplitude  
Moat on the edge of highs  
Background: parallel to subparallel  
Length: 10->70s km  
Height: 10->400 msTWT

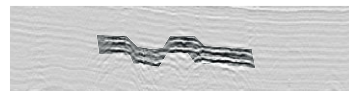
(e) **Sheeted/abyssal drift**



Sheet / low to high amplitude  
Background: parallel to subparallel  
Length: 10->100s km  
Height: 10-100 msTWT

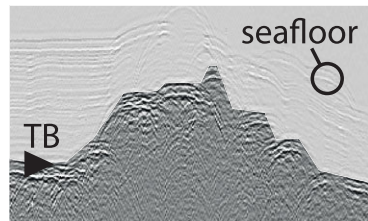
Vertical exaggeration in sediments ~x11 and in volcanics ~x4,4

(f) **Volcanic sill**



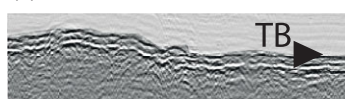
Single event / high amplitude  
Cross-cutting reflection  
Background: parallel to subparallel  
Length: 0,5-5,5 km  
Height: 0,2-0,4 sTWT

(g) **Volcanic mound**



Mound / Top: high amplitude, disrupted.  
Overlying: onlap or concordant  
No base  
Length: 1->10s km  
Height: 0,2->1,4 sTWT

(h) **Oceanic crust / acoustic basement**



Single event / high amplitude  
Overlying: onlap or concordant  
Background: parallel to subparallel

**Fig. 3.** (Colour online) Seismic facies observed in the study area between the acoustic basement (TB – top basement) and the seafloor. Two main seismic facies classes, volcanic rocks and sedimentary, are observed within the study area and interpreted based on Calvès et al. (2011), and Dubois & Mitchell (2012) and Rebesco et al. (2014), respectively. TWT – two-way time.

considered in this study and the angle of subduction and bending changes slowly over long periods of geologic time, but this is not thought to affect the interpretation of the drift presented here. The SW Nazca Ridge shows numerous volcanic mounds and seamounts (Fig. 2a, inset  $\beta$ ; Fig. 2b). Towards the northeast, the seafloor of the Nazca Ridge shows fewer bathymetric highs related to volcanic features compared to the southwestern part (Fig. 2b; Hampel *et al.* 2004). The Nazca Ridge shows the seafloor geomorphology of an oceanic plateau (Harris *et al.* 2014; Fig. 2b), is narrow in the southwest (c. 156 km) and wider towards the northeast (c. 296 km). The seafloor is smoother in the same direction reflecting the thicker sediment cover present to the northeast (Fig. 2a, inset  $\gamma$ ; Fig. 2b). Nonetheless, the smooth seafloor is also affected by incisions that are oriented perpendicular to the Nazca Ridge axis (Fig. 2a, inset  $\gamma$ ) and that mark abyssal erosion linked to bottom current activity (Lonsdale, 1976; Land *et al.* 1999; Gomes & Viana, 2002; Dubois & Mitchell, 2012; Mitchell & Huthnance, 2013; Rebesco *et al.* 2014; Juan *et al.* 2018). The relative importance of physical erosion and carbonate dissolution below the carbonate compensation depth (CCD) cannot be clearly resolved (Lonsdale, 1976).

### 3.b. Seismic facies

Although numerous different seismic facies schemes have been proposed in the literature, these typically share many similarities (e.g. Rebesco & Stow, 2001; Stow *et al.* 2002; Donda *et al.* 2003; Nielsen *et al.* 2008; Ryan *et al.* 2009; Boyle *et al.* 2017). We opt to use the scheme of Faugères *et al.* (1999), because it addresses all the different seismic patterns seen in this work and alternatives do not provide a significant advance in this case. Two main seismic facies classes are observed within the study area. The first class comprises reflectors interpreted as volcanic features, such as volcanic mounds, volcanic sills and the oceanic basement itself (Fig. 3). The second class is interpreted as deep-water sedimentary facies linked to the bottom currents observed to flow along the upper slopes of seamounts towards abyssal basins (Fig. 3).

The oceanic basement facies is encompassed by a single high amplitude reflection with minor to major offset related to faults (Fig. 3). This regional facies is locally affected by topographic highs that are associated with volcanic mounds (Fig. 3). The mounds have a variety of heights and slopes with steep or steepened flanks. These volcanic mounds have very low amplitude chaotic internal facies with rare high amplitude reflections. Most of these mounds are partially or completely buried under the concordant to onlapping parallel seismic facies described below. A cross-cutting high amplitude facies is present in the sedimentary cover above the acoustic basement. This high amplitude, saucer-shaped facies is interpreted to be indicative of volcanic sills (Planke *et al.* 2005; Magee *et al.* 2013) (Fig. 3). The other observed facies are all within the seismic sequence spanning between the acoustic basement/oceanic crust and the seafloor. The most extensive facies developed regionally above the oceanic crust is the sheeted abyssal drift (Figs 3e, 4) that is characterized by parallel-concordant low to high amplitude reflections. The drift is mainly present in the two oceanic basins of Peru and Chile and in the Peru–Chile Trench where it is cut by faults (Fig. 4a). This facies was drilled at Deep Sea Drilling Project (DSDP) Site 321/ODP Site 1231 in the northern Peru Basin (Fig. 1) where it comprises fine-grained sediments, such as hemipelagic clay rich in siliceous fossils, discrete tephra horizons and dispersed volcanic ash, as well as nannofossil ooze interbedded

with iron-rich nannofossil ooze (Shipboard Scientific Party, 1976, 2003b).

Four other seismic facies are observed in shallower layers of the SE Pacific Ocean. The first has low amplitude reflections in seismic data, with edges marked by a moat and wavy to parallel reflections. This facies is typical of a plastered drift (Fig. 3a; e.g. Faugères *et al.* 1999) and is mainly observed on the edge of the Nazca Ridge (Fig. 4b, c). On the edge of some volcanic mounds, this facies has a mounded morphology, with low internal amplitudes that show an aggrading stack towards the flank of the topographic highs and thinning towards the external part of the mound. Parallel reflections are observed at the base of the mound and wavy reflections towards its upper surface. A small depression is observed along the contact between the mound edge and the supporting underlying structure. This mounded facies is associated with a moat (Fig. 3b). Mounded features, isolated from the main Nazca Ridge (i.e. separated), show basal terminations that are onlapping or downlapping. When the mounds lie adjacent to a bathymetric high they show a depressed upper surface ('moat' or contourite channel), which is aggrading and migrating upslope. Therefore, we interpret these features as a mounded separated/isolated drift following the scheme of Faugères *et al.* (1999). Where two topographic/basement highs are present, mounded features with low to high amplitude, parallel to wavy internal reflection are observed with moats in seismic data at their edges. These types of structures are typical of a confined drift (Fig. 3c; e.g. Faugères *et al.* 1999; Bailey *et al.* 2021). The thickest and most extensive facies is typically a mounded-wedge of sediments with low seismic amplitude, with a moat along the edge of the mound and with parallel to sub-parallel internal reflections. This facies is identified as a fault/scarp-controlled drift because of its link to the steep, fault-bounded slopes of the Nazca Ridge (Fig. 3d; e.g. Rebesco & Stow, 2001 and references therein). This facies is present between the Nazca Ridge top and the edge of the ridge (Fig. 4). This facies transitions away from the ridge into thinner bedded facies such as the sheeted abyssal drift (Fig. 4). In the following section the facies related to bottom currents are identified on a regional section (Fig. 4a–c) and combined with a thickness map of the sedimentary pile to define the Nazca Drift System (Fig. 4d).

### 3.c. Nazca Drift System

Various seismic facies are observed within the complete sedimentary column between the top of the oceanic crust and/or Nazca Ridge (top basement) and the seafloor (Figs 3, 4a–c). The Nazca Drift System extends over the whole study area, with thickness varying from c. 104 m on the SW flank of the Nazca Ridge at  $\sim 18^\circ$  N to 375 m on the top of the ridge offshore southern Peru (Fig. 4d). Within this sequence the main depocentre is located in the NE part of the Nazca Ridge (north of  $18^\circ$  S) and extends from SW to NE (Fig. 4a, d), reaching a maximum thickness in the Peru–Chile Trench. From the Nazca Fracture Zone to the Peru Basin, the sequence thickens above the Nazca Ridge (Fig. 4b, d). The minimum thickness of this sequence is observed in the northern part of the Peru Basin (Fig. 4c, d). Locally the sequence is very thin, especially on the slopes of seamounts and volcanic mounds (Fig. 4a–c). The oceanic crust in the study area spans an age of 45 Ma on the edge of the Peru–Chile Trench to younger than 32 Ma southwest of the Nazca Ridge (Hampel, 2002; Müller *et al.* 2008). At ODP Site 1237 the oldest strata cored are Oligocene, with an age of c. 31 Ma (Shipboard Scientific Party,

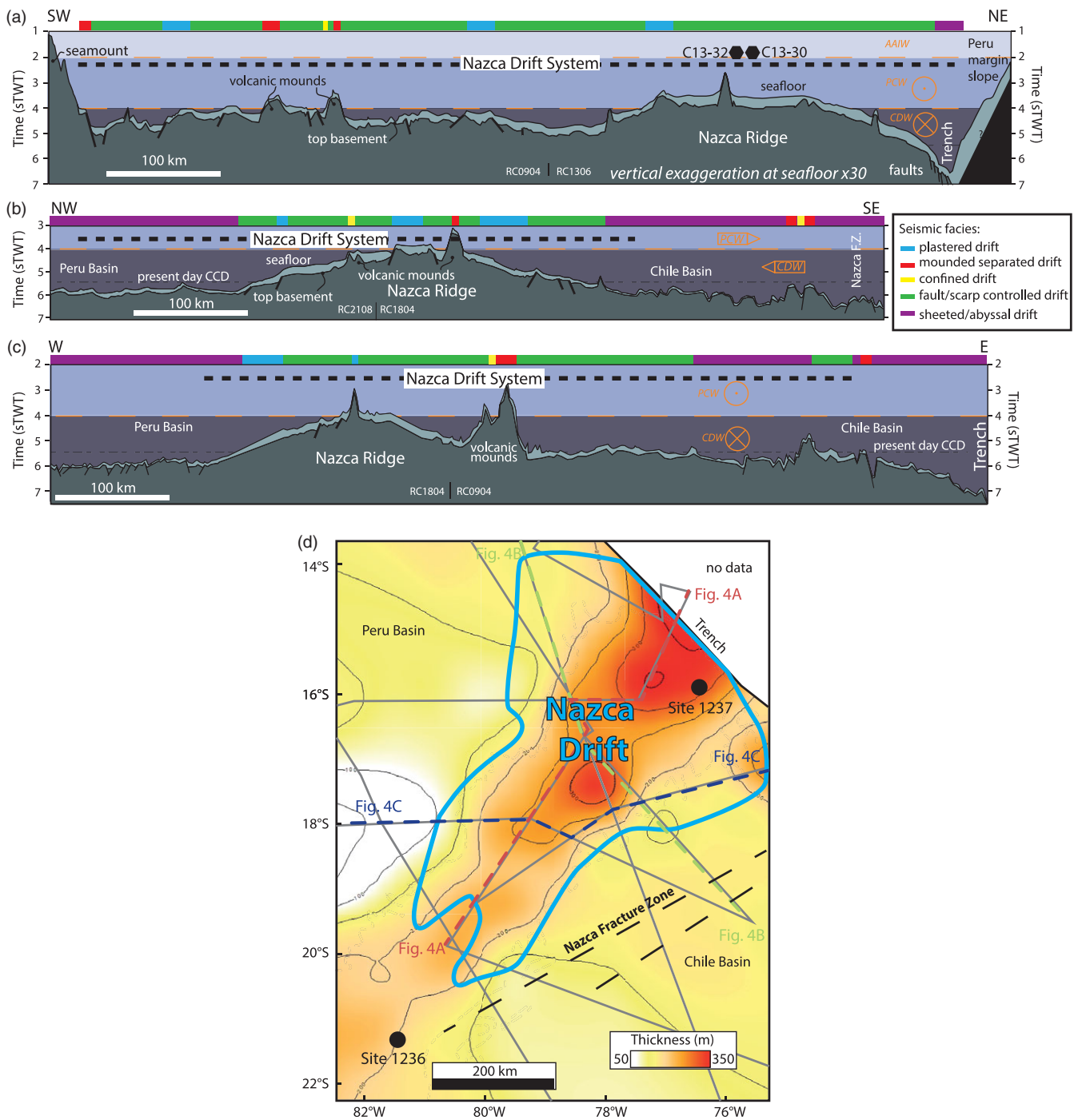


**Fig. 4.** (Colour online) Regional line drawing of seismic reflection lines (single channel seismic: SCS, LDEO) across the Nazca Ridge and the Nazca Drift System. (a) From seamount SW of Nazca Ridge to the Peru–Chile Trench (SW–NE). (b) From Peru Basin across the Nazca Ridge to the Chile Basin and the Nazca Fracture Zone (NW–SE). (c) From the Peru Basin to the Chile basin and Peru–Chile Trench (W–E). (d) Isopach map of megasequence above acoustic basement. AAIW – Antarctic Intermediate Water; CDW – Circumpolar Deep Water; PCW – Pacific Central Water; CCD – carbonate compensation depth.

2003a; King & Wade, 2017). The basement was not reached at that location.

**4. Discussion**

**4.a. Regional stratigraphy**

The Nazca Drift, which spans c. 500 km by 850 km, compares with other major drift systems worldwide. The Meiji Drift in the North

Pacific is up to 1800 m thick, over 1000 km long and c. 350 km wide (Kerr *et al.* 2005). The Gardar Drift of the North Atlantic extends for 1100 km, while the smaller Bjorn and Eirik drifts are 300 and 650 km long each and reach thicknesses of 720 and 1400 m, respectively (Parnell-Turner *et al.* 2015). The carbonate affiliated Pourtales Drift of the Bahamas Bank–Florida margin runs for c. 400 km and is 30 km across and c. 500 m thick (Mulder *et al.* 2019); the nearby confined Sarenten Drift (200 by 60 km) is more than 1000 m thick (K. L. Bergman, unpub. Ph.D. thesis, Univ.

Miami, 2005). The confined Sumba Drift in Indonesia is more than 1000 m thick but only *c.* 20 km wide by 120 km long (Reed *et al.* 1987). Likewise, the confined Faro Drift in the Gulf of Cadiz extends for 80 km and reaches thicknesses of 600 m (Stow *et al.* 2002). Intermediate sized drifts in the SW Pacific, the Chatham and Rekohu drifts, are 300 and 250 km long and are 400 and 480 m thick, respectively (Carter & McCave, 1994, 2002; Bailey *et al.* 2021).

We interpret the Nazca Drift System based on the occurrence of seismic facies related to bottom currents, the thickness of the entire sequence and seafloor geometry. Its SW extent is presently not well defined because of the absence of regional seismic profiles in this part of the study area. Confined drift facies between and along the slopes of volcanic mounds in the southwest of the study area are observed at ODP Site 1236, but we limit the Nazca Drift System to being northwest of this area because a connection is not possible to establish at present as a result of the barrier created by the seamount southwest of the Nazca Ridge (Fig. 4a, d).

We rule out significant sedimentation in the form of carbonate platforms because of their distinctive shape on seismic, which is not observed in this case (cf. K. L. Bergman, unpub. Ph.D. thesis, Univ. Miami, 2005; Mulder *et al.* 2019), while core analysis confirms low volcanic input. Some of the material at ODP Site 1237 may have been transported by Trade Winds from the Atacama Desert, but this would be less important further south and further offshore. Evenly spread aeolian dust would not originally form the thickness variations mapped in the seismic but could be reworked by bottom currents. Mass wasting can be excluded based on the lack of seismically homogeneous intervals that characterize this type of sedimentation. The Nazca Drift System is pear-shaped in plan-view, with its widest part located at the Peru–Chile Trench (Fig. 4d). The facies mapped along the three regional cross-sections (Fig. 4a–c) show the dominant types related to extensive fault scarp-controlled drift sedimentation. In transition to the sheeted abyssal drift facies in the abyssal deepest part of the oceanic bounding basins, plastered drift facies are observed on slopes on both sides of the Nazca Ridge (Fig. 4b, c).

The Nazca Drift System presently sits in water depths of 2090–5330 m (Fig. 5a). Erosional surfaces at the seafloor marked by top-laps and erosional truncations are observed on 2D seismic profiles at water depths of *c.* 2200–4095 m. Figure 5b shows how the top-laps and erosional truncations are preferentially found in this water depth range, especially 2500–3000 m, implying frequent submarine erosion driven by bottom currents. This range of water depths leaves most of the upper surface of the Nazca Drift System exposed to the present-day PCW and CDW (Fig. 5c). The asymmetric thickness of the Nazca Drift System, i.e. thinner in the Chile Basin compared to the Peru Basin, could be explained by northward movement of the CDW (Lonsdale, 1976).

The Nazca Drift System covers an area of 204 500 km<sup>2</sup>. It represents the largest yet identified abyssal drift system in the Pacific Ocean. Globally it is only surpassed by the Zapiola Drift in the western South Atlantic and the Mozambique Channel contourite in the Indian Ocean (Kolla *et al.* 1980; Flood & Shor, 1988; Rebesco *et al.* 2014). The volume of this giant sedimentary body is *c.* 51 445 ± 5715 km<sup>3</sup> (Fig. 4d). If the Nazca Drift System is no older than Oligocene, the average long-term accumulation rate is 0.7 ± 0.08 km<sup>3</sup> ka<sup>-1</sup>. This is more than the *c.* 0.14 km<sup>3</sup> ka<sup>-1</sup> estimated for the Faro Drift since Miocene time (Stow *et al.* 2002), but comparable with values of 0.74 to 1.31 km<sup>3</sup> ka<sup>-1</sup> in drifts offshore Newfoundland since Eocene time (Boyle *et al.* 2017), or 0.88 km<sup>3</sup> ka<sup>-1</sup> in the Snorri Drift and 1.07 km<sup>3</sup> ka<sup>-1</sup> in the

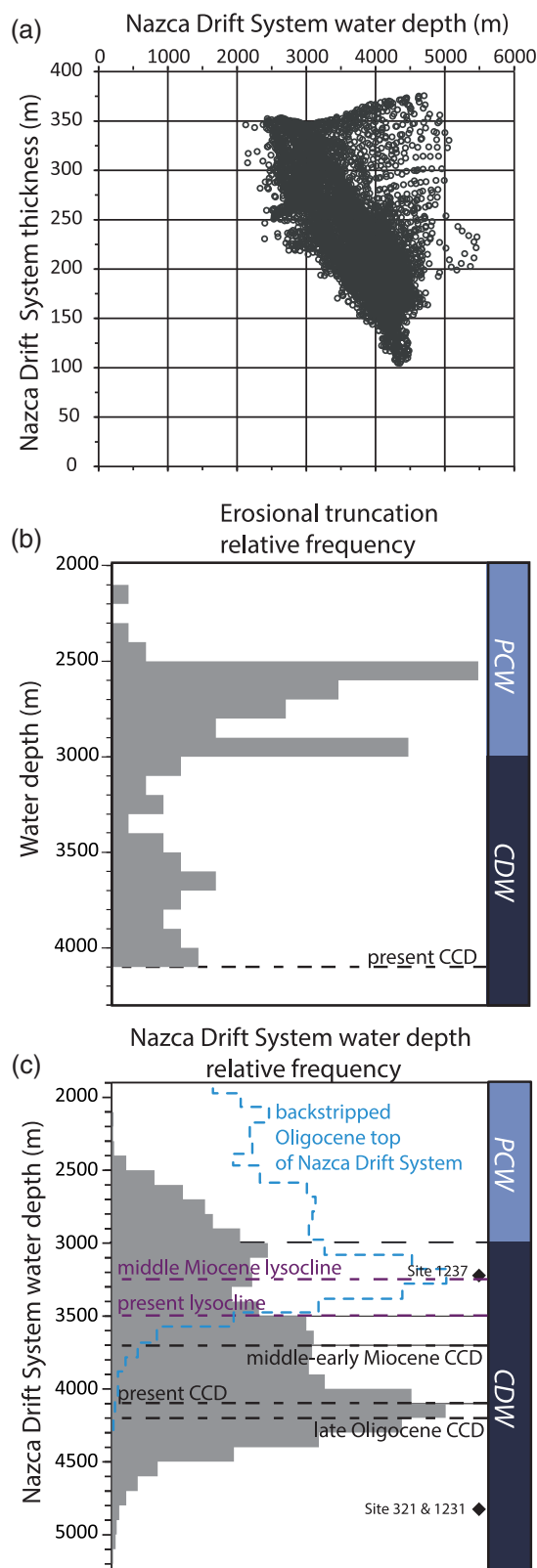


**Fig. 5.** (Colour online) Hypsometry of Nazca Drift System present-day drift with palaeoceanography framework and present-day water masses. (a) Scatter plot of Nazca Drift System thickness as a function of water depth; (b) Nazca Drift System erosional truncation relative frequency by water depth range; and (c) Nazca Drift System water depth relative frequency. Present-day, palaeo-carbonate compensation depth (CCD) and lysocline in the South Pacific Ocean (Rea & Leinen, 1985). Pacific Central Water (PCW) and Circumpolar Deep Water (CDW) (Tsuchiya & Talley, 1998). Depths of DSDP and ODP sites are present-day water depth at each site (Shipboard Scientific Party, 1976, 2003a).



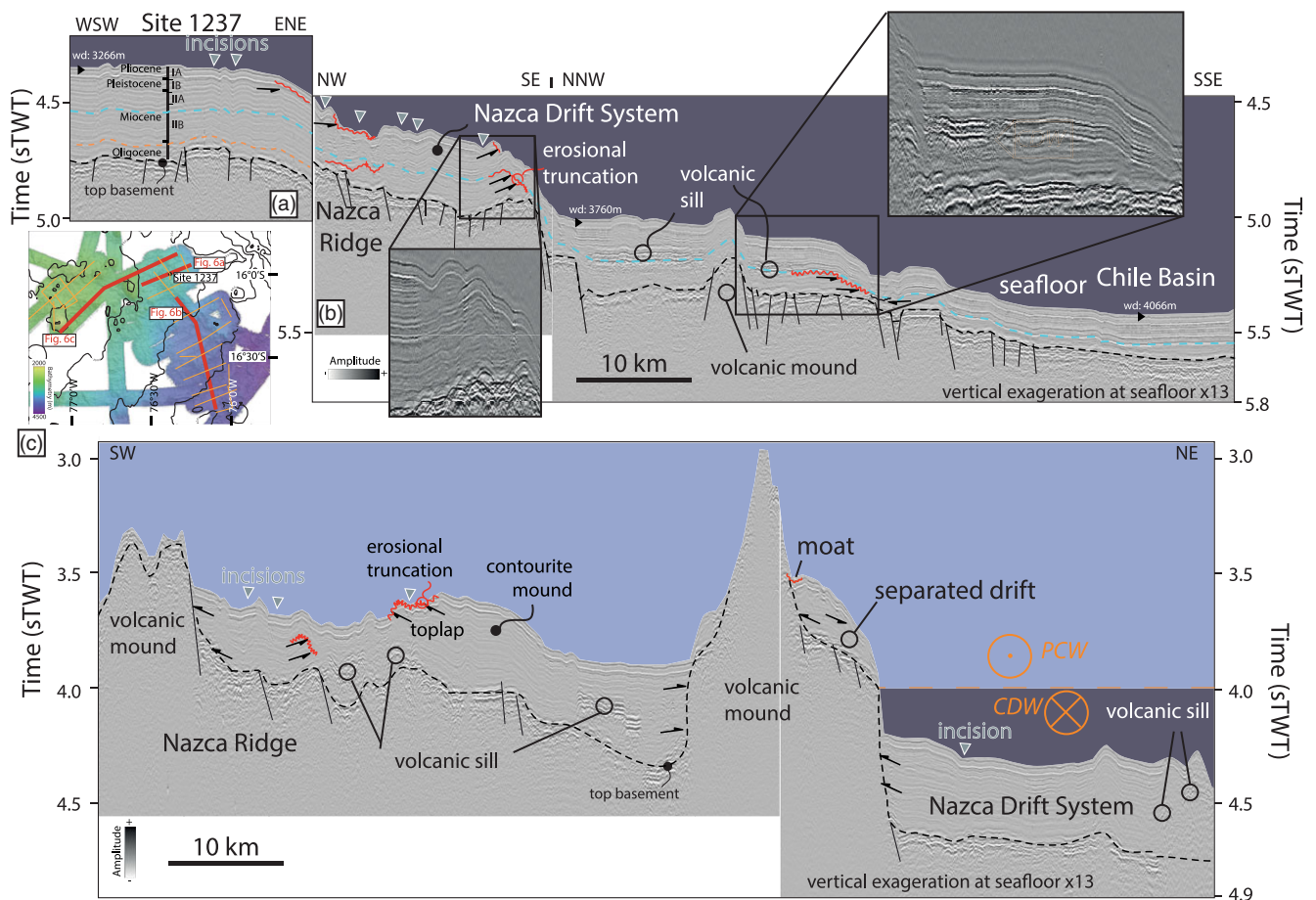


**Fig. 6.** (Colour online) Eastern Nazca Drift System seismic framework. (a) WSW–ENE seismic profile across ODP Site 1237 with stratigraphy (Shipboard Scientific Party, 2003a); (b) NW–SSE seismic profile from the Nazca Ridge to the Chile Basin; and (c) SW–NE seismic profile along the long axis of the Nazca Ridge with volcanic mounds and varying thickness of the Nazca Drift System. Note the volcanic sill intruding the Nazca Drift System. Location of the profiles is in the bathymetry inset map, where the blue line shows the extent of the seismic surface used to calibrate the age of the buried unconformities related to the erosional truncations. Water masses and current directions are layered above the acoustic seafloor. Pacific Central Water (PCW) and Circumpolar Deep Water (CDW) (Tsuchiya & Talley, 1998).

Hatton Drift (Wold, 1994) of the NE Atlantic. It is, however, somewhat less than the  $13.6 \text{ km}^3 \text{ ka}^{-1}$  and  $7.94 \text{ km}^3 \text{ ka}^{-1}$  estimated for the Eirik and Gardar drifts of the NE Atlantic.

#### 4.b. Chronological framework

Unconformities are observed at the seafloor and within the subsurface of the Nazca Drift System (Figs 5b, 6). The seafloor is affected by erosion, and the underlying Plio-Pleistocene strata are also marked by erosional truncation at various water depths (Figs 5b, 6). The seafloor water depth at which the transition from the southward migrating PCW and northward migrating CDW occurs is correlative of these erosional truncations (Fig. 4b). These erosive surfaces in the NE part of the Nazca Drift System have scoured geometries, with orientations suggesting they were produced by SE to NW flow (Figs 2, 6). These subsurface unconformities are localized in areas where the sedimentary section is draping fault scarps that offset the basement and have significant heave ( $>125 \text{ ms}$  two-way time (TWT)). Mass wasting is not thought to be significant because it has a very distinctive seismic character, with thick, homogeneous units quite the opposite of the laminated facies seen here. Mass wasting in ocean island settings is moreover generally restricted to the time immediately after eruption and not the long time intervals seen here (e.g. Rees *et al.* 1993; Wolfe *et al.*

1994). The ages measured at ODP Site 1237 allows calibration of the duration of the oldest unconformities observed in the SE part of the drift where they are projected on seismic lines (Fig. 6a, b). The older age is estimated at the depth of the mid to upper Miocene, and the youngest sediment above this truncation is associated with the intra-upper Miocene. The top of the unconformity is bracketed at a depth of 149–170 m below seafloor, based on P wave velocity ranging from 1600 to  $1800 \text{ m s}^{-1}$ . The youngest calibrated age for the unconformity from the shipboard age model of ODP Site 1237 is from *c.* 7.7 to 9.4 Ma (Shipboard Scientific Party, 2003a).

The unconformities do not seem to be associated with mass wasting because there is no scarp up-dip or chaotic/transparent seismic facies diagnostic of mass transport deposits identified down slope of the unconformity regions. The high carbonate content of sediment described at ODP Site 1237 excludes strong dissolution as a cause of the unconformities driven by sedimentation below the CCD (Berger, 1978; Berger *et al.* 1982), thus making the erosional truncations likely to have been caused by remobilization of the exposed parts of the Nazca Drift System caused by intense bottom current scouring, potentially active over long periods of time (Heezen & Hollister, 1964; Southard *et al.* 1971; Bornhold & Summerhayes, 1977; Marani *et al.* 1993). No bottom current velocity has been measured at the Nazca Ridge, but instead further north at the Carnegie Ridge (Lonsdale & Malfait, 1974) and south

of it in the Chile Basin (Shaffer *et al.* 1995, 2004), where bottom water is flowing at mean speeds of from 3 to 7.8 cm s<sup>-1</sup>. Lonsdale (1976) suggested the presence of rather slow currents east and west of the Nazca Ridge, in the sill and trench where water moving from the Chile to the Peru Basin is flowing at depths deeper than the adiabatic bottom layer. Furthermore, the measured tidal currents (15–20 cm s<sup>-1</sup>) at the Carnegie Ridge are superimposed with slow speed drift (3 cm s<sup>-1</sup>). This abyssal tidal current is effective at driving erosion of fine particles (Lonsdale & Malfait, 1974). By analogy with the Carnegie Ridge, the study area would be prone to being influenced by the same processes, tidal forcing and strong bottom currents, causing erosion at the seafloor surface. Current-driven erosion of the seafloor at depths of ~2 km is also known immediately north of the Nazca Ridge in the Lima Basin (Clift *et al.* 2003). Experimental erosion of calcareous ooze by currents showed that the critical speed for erosion to start is *c.* 7–10 cm s<sup>-1</sup> (Southard *et al.* 1971), corresponding to the observed values of near bottom currents in the SE Pacific.

#### 4.c. Initiation of the Nazca Drift System in the regional oceanic gateways framework

The Nazca Drift System extends from the southwest of the Nazca Ridge to the Peru–Chile Trench (Fig. 4). The eastward motion of the Nazca Plate since the emplacement of the drift is well constrained (e.g. Hampel, 2002). Before the Nazca Ridge reached the trench, normal, low-relief oceanic crust had been subducting. The trench-slope of South America and the oceanic barrier formed by the Nazca Ridge against bottom waters moving from the Southern Ocean to the equatorial domain results in a funnel for sediment transport. The oldest sediments cored at ODP Site 1237 (*c.* 31 Ma; King & Wade, 2017) indicate carbonate sedimentation until 15 Ma (Fig. 7a). The basement was not reached by drilling at ODP Site 1237, but the sediment column between the total drilled depth and the acoustic basement is thin (0.016 s TWT *c.* 15 m; Fig. 6), implying a maximum age of *c.* 36.8 Ma at the base (sedimentation rate of 2.55 m Ma<sup>-1</sup>; King & Wade, 2017), which is younger than the initiation of the opening of the Drake Passage (41 Ma; Scher & Martin, 2006). The initiation of the Nazca Drift System could be related to the opening of the Drake Passage and the northward branch bifurcation of the ACC along the Pacific margin of South America (Lawver & Gahagan, 1998; Hodel *et al.* 2021).

Supply of the main fraction of the sediments composing the Nazca Drift System is related to the evolution of water masses and currents. As a result, the sedimentation rate must partly reflect the signal of the current intensity, as well as sediment supply rate. The clastic input is a reflection of the proximity of the ridge to terrestrial sources, mainly dust (aeolian siliciclastic), while migrating towards South America (Tiedemann & Mix, 2007). The averaged sedimentation rate over 1 million-year intervals at ODP Site 1237 (Fig. 7a) in the eastern portion of the Nazca Drift System increased during the period when the discontinuity is recorded at 9.4–7.0 Ma on the seismic profile. Sediment was eroded where the discontinuity is seen and transported and deposited in the region of ODP Site 1237. The thickness of the drift is higher to the north of where the intra-Miocene unconformity is developed on the side of the ridge (Fig. 6) because the bottom current related to the CDW sweeps sediments towards ODP Site 1237. About 70% of the Nazca Drift System is above the CCD at the present day (Figs 4, 5c). Reconstructions based on a typical rate of oceanic subsidence

(Stein & Stein, 1992) indicate that ODP Site 1237 on the Nazca Ridge would have been above the regional CCD until 21.7 Ma (Fig. 7; Rea & Leinen, 1985; Pälke *et al.* 2012). DSDP Site 321 in the abyssal Peru Basin north of the study area descended below the CCD after 24 Ma (Fig. 7b; Rea & Leinen, 1985). ODP Site 1237 is shallower and crossed the CCD during early Miocene time. The CaCO<sub>3</sub> mass accumulation rates had been stable for over *c.* 2 million years before decreasing after 20 Ma and increased again towards the end of middle Miocene time at *c.* 12 Ma (Fig. 7a, b). This framework excludes a major role for carbonate dissolution in the generation of unconformities within or above the Nazca Drift System. The CCD could have been locally depressed by high deposition rates, as observed at the equator (Pälke *et al.* 2012).

#### 4.d. Intensity of bottom water flow and building the Nazca Drift System

The thickness variation and identification of internal and superficial unconformities within the Nazca Drift System shows that bottom water currents have played a key role in the evolution of the sedimentary record in this part of the Pacific Ocean.

Framed within the last 30 Ma, the study area has been under the influence of Southern Ocean evolution, as well as solid earth and hydrosphere interaction (e.g. Scher *et al.* 2015; Wright *et al.* 2016) (Fig. 7c). Similar to the Eastern New Zealand Oceanic Sedimentary System, which is made of abyssal drift deposits (Carter *et al.* 1996; Carter & McCave, 1994, 2002; Bailey *et al.* 2021), the Nazca Drift System has been emplaced in an abyssal domain since Oligocene time under the influence of the ACC and the associated CDW. The oldest Oligocene sequences drilled at ODP Site 1237 record alternating fine-scale variations and changes in sedimentation rates that started with the lowest rate operating over periods of *c.* 3.6 million years (before 29.8 and 28.2–24 Ma) and higher rates during shorter periods of 1.6 million years (29.8–28.2 Ma and 24–21.5 Ma) (King & Wade, 2017). These changing rates could reflect the intensity of sediment supply to the ocean and/or variation in the intensity of bottom currents.

A widespread erosional event associated with the establishment of the ACC and the Deep Western Boundary Current has been identified in the record of the Bounty Trough – SW Pacific Ocean (Horn & Uenzelmann-Neben, 2015). A major *c.* 5 million-year hiatus separates the middle Miocene, *c.* 10.4 Ma, from the lower Pliocene at ODP Site 1122 (Shipboard Scientific Party, 1999; Carter *et al.* 1999). This erosional event correlates with the intensification caused by a more vigorous ACC, synchronous with the build-up of the West Antarctic Ice Sheet (Carter *et al.* 2004). In the Drake Passage, the identified South Falkland Slope Drift also contains unconformities of the same age, *c.* 9 Ma (Koenitz *et al.* 2008). The thickness of the drift is a function of the evolution of sediment supply and current intensity. High sedimentation rates in early Miocene time were followed by a decreasing rate during mid–late Miocene time, followed by a late Miocene peak and further decline from the late Miocene to the Pleistocene period. The identified unconformity within the Nazca Drift System is dated within this middle Miocene period of intensified bottom currents, *c.* 7.7–9.4 Ma. We therefore attribute this unconformity to the same process. Geochemical analyses at ODP Site 1237 show a change in nutrient burial preservation from oxygenated to more reduced conditions at *c.* 162 m composite depth (8.8 Ma; Chun & Delaney, 2006). This change corresponds to the depth at which the late Miocene

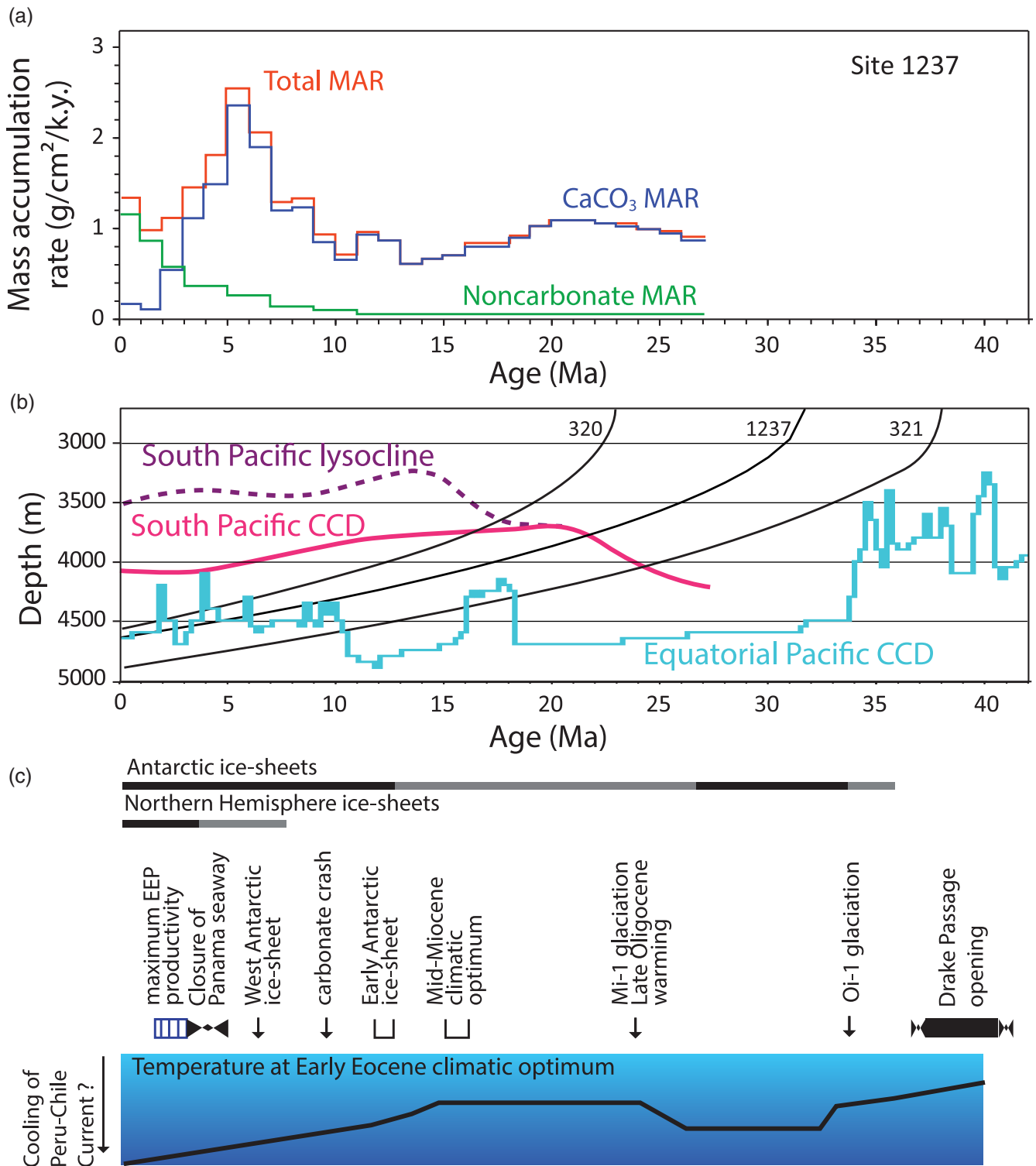


**Fig. 7.** (Colour online) (a) Sedimentation rate at ODP Site 1237 (Shipboard Scientific Party, 2003a) and (b) subsidence at three DSDP and ODP sites with carbonate compensation depth (CCD) and lysocline depths over the last 40 million years in two domains of the Pacific Ocean (Rea & Leinen, 1985; Pälike *et al.* 2012). (c) Palaeoceanography, geodynamic and climatic context sourced from Zachos *et al.* (2001), Lamb & Davies (2003) and Scher & Martin (2006).

unconformity was identified on seismic reflection profiles and could be attributed to bottom water chemistry and variations in current activity in this part of the SE Pacific Ocean. The ACC strength has been documented further south, with initiation dated to have occurred during late Oligocene to late Miocene times (Lyle *et al.* 2007).

**4.e. Tectonic and contourite drift in the subduction channel**

A significant part of the Nazca Ridge has been subducted since at least the end of middle Miocene time, *c.* 11.2 Ma (Hampel, 2002). Because ridge construction and the sedimentary drift accumulation are older than the initiation of Nazca Ridge subduction, a

potentially large volume of deep-sea sediments and polymetallic accumulations could have contributed to orogenesis and mineralization in the Andes.

Water is widely recognized to be a key ingredient in the generation of magmas in subduction zones, making these zones efficient areas of carbon burial (Grove *et al.* 2012; Clift, 2017; Plank & Manning, 2019). Geodynamic reconstructions indicate that metallogenesis has followed the southward movement of the Nazca Ridge along the coast of South America (Rosenbaum *et al.* 2005). This migration is associated with an increase in emplacement of Cu, Au and Zn deposits from 8 to 6 Ma (Rosenbaum *et al.* 2005). The area of the Nazca Ridge that has subducted since 11.2 Ma is estimated to represent an area of  $c. 420 \times 10^3 \text{ km}^2$ . This subducted part of the plate was covered by sediments, similar to the remaining western part of the Nazca Ridge. We estimate, based on the present-day thickness of Oligocene–middle Miocene strata (Fig. 6a; 0.225 s TWT) that the maximum subducted sediment thickness was 180–200 m. This results in a figure of  $80 \pm 5 \times 10^3 \text{ km}^3$  of sediments that may have contributed to Andean mineral evolution. The porosity of this sedimentary sequence can be high at 60–90 % (Velde, 1996; D'Hondt *et al.* 2003; Yu *et al.* 2020), leading to a higher than normal amount of water entering the subduction channel (Bray & Karig, 1985), especially considering that subduction of the Nazca Ridge increased subduction erosion along the Andean margin, adding even more sediment and water from any pre-existing accretionary prism (Clift *et al.* 2003; Kukowski & Oncken, 2006). This higher volume of water at the Nazca Ridge could have increased the amount of melting.

## 5. Conclusions

Based on seafloor bathymetry, seismic reflection data and scientific drilling sites, we conclude that the Nazca Drift System has been identified in the SE Pacific Ocean. The Nazca Drift System spans from the Chile Basin, across the Nazca Ridge into the Peru Basin. This major palaeoceanographic sedimentary feature in the SE Pacific Ocean has accumulated on top of the Nazca Ridge since Oligocene time. The Nazca Drift System represents the largest identified abyssal drift system yet known in the Pacific Ocean, and formed because of the primary present-day bottom currents winnowing the seafloor sediments of the Nazca Drift System. These currents are related to the PCW and CDW. Initiation of the Nazca Drift System may have been related to the opening of the Drake Passage and the northward branch bifurcation of the ACC along the Pacific margin of South America.

The currents that have sculpted this giant sedimentary body experienced fluctuating intensities, as recorded by internal unconformities identified by acoustic discontinuities. The calibrated age of the oldest unconformity in the SE part of the Nazca Drift System is late Miocene (Tortonian) and can be correlated to the change of bottom water conditions recorded at ODP Site 1237 from oxygenated to more reduced conditions. Evidence of younger discontinuities shows that the bottom currents have been varying in response to southern hemisphere climatic change and the eastward motion of the Nazca Plate. A significant part of the Nazca Drift System that has already subducted has contributed material to the subduction channel. This is further spatially related onshore to subduction magmatism and mineralization, as well as the Andean orogenic cycle since late Miocene time (*c.* 11.2 Ma).

Further analyses such as grain size and geochemistry should be able to constrain the palaeo-bottom current intensity, variations and the detailed emplacement of this sedimentary drift. Future

studies comparing these findings to drift systems developed along other deep-water active margins will lead to recognition of an increasing number of new drift system provinces.

**Supplementary material.** To view supplementary material for this article, please visit <https://doi.org/10.1017/S0016756821000960>

**Acknowledgements.** This research used data provided by the International Ocean Discovery Program (IODP). GENE03RR subsurface data were accessed by the Site Survey Data Bank (SSDB, <https://ssdb.iodp.org/index.php>). Cecily Pálíke (MARUM) and Peggy Delaney (UCSC) are thanked for discussion regarding the geochemistry of sediments at Site 1237. Andrea Hampel (Leibniz Universität Hannover) is thanked for access to the velocity data from the SO146-GEOPECO cruise. Paul Henkart is thanked for help with the single channel data. NOAA-NCEI is thanked for the Multibeam Bathymetry database (<https://www.ngdc.noaa.gov/maps/autogrid/>). IHS-Kingdom is thanked for their Software University Grants that have allowed this work to take place. Thanks to Neil Mitchell (University of Manchester) and an anonymous reviewer for commenting on an earlier version of our manuscript. Reviews from the editor Stephen Hubbard, and reviews from W. Bailey, M. Cason, F. J. Hernández-Molina and an anonymous reviewer greatly helped to clarify our work.

**Conflict of Interest.** The authors declare that they have no conflict of interest.

## References

- Bailey WS, McArthur AD and McCaffrey WD (2021) Distribution of contourite drifts on convergent margins: examples from the Hikurangi subduction margin of New Zealand. *Sedimentology* **68**, 294–323. doi: [10.1111/sed.12779](https://doi.org/10.1111/sed.12779).
- Barker PF, Filippelli GM, Florindo F, Martin EE and Scher HD (2007) Onset and role of the Antarctic Circumpolar Current. *Deep Sea Research Part II: Topical Studies in Oceanography* **54**, 2388–98. doi: [10.1016/j.dsr2.2007.07.028](https://doi.org/10.1016/j.dsr2.2007.07.028).
- Berger WH (1978) Sedimentation of deep-sea carbonate; maps and models of variations and fluctuations. *Journal of Foraminiferal Research* **8**, 286–302. doi: [10.2113/gsjfr.8.4.286](https://doi.org/10.2113/gsjfr.8.4.286).
- Berger WH, Bonneau M-C and Parker FL (1982) Foraminifera on the deep-sea floor: lysocline and dissolution rate. *Oceanologica Acta* **5**, 249–58.
- Bornhold BD and Summerhayes CP (1977) Scour and deposition at the foot of the Walvis Ridge in the northernmost Cape Basin, South Atlantic. *Deep Sea Research* **24**, 743–52. doi: [10.1016/0146-6291\(77\)90497-0](https://doi.org/10.1016/0146-6291(77)90497-0).
- Boyer TP, Antonov JJ, Baranova OK, Coleman C, Garcia HE, Grodsky A, Johnson DR, Locarnini RA, Mishonov AV, O'Brien TD, Paver CR, Reagan JR, Seidov D, Smolyar IV and Zweng MM (2013) *World Ocean Database 2013*; NOAA Atlas NESDIS 72 (ed. S Levitus; technical ed. A Mishonov). Silver Spring, MD: National Oceanographic Data Center, 209 pp. doi: [10.7289/V5NZ85MT](https://doi.org/10.7289/V5NZ85MT).
- Boyle PR, Romans BW, Tucholke BE, Norris RD, Swift SA and Sexton PF (2017) Cenozoic North Atlantic deep circulation history recorded in contourite drifts, offshore Newfoundland, Canada. *Marine Geology* **385**, 185–203. doi: [10.1016/j.margeo.2016.12.014](https://doi.org/10.1016/j.margeo.2016.12.014).
- Bray CJ and Karig DE (1985) Porosity of sediments in accretionary prisms and some implications for dewatering processes. *Journal of Geophysical Research: Solid Earth* **90**, 768–78. doi: [10.1029/JB090iB01p00768](https://doi.org/10.1029/JB090iB01p00768).
- Calvès G, Auguy C, de Lavaissière L, Brusset S, Calderon Y and Baby P (2017) Fore-arc seafloor unconformities and geology: insight from 3-D seismic geomorphology analysis, Peru. *Geochemistry, Geophysics, Geosystems* **18**, 3062–77. doi: [10.1002/2017GC007036](https://doi.org/10.1002/2017GC007036).
- Calvès G, Schwab AM, Huuse M, Clift PD, Gaina C, Jolley D, Tabrez AR and Inam A (2011) Seismic volcanostratigraphy of the western Indian rifted margin: the pre-Deccan igneous province. *Journal of Geophysical Research* **116**, B01101. doi: [10.1029/2010JB008082](https://doi.org/10.1029/2010JB008082).
- Carter L, Carter RM and McCave IN (2004) Evolution of the sedimentary system beneath the deep Pacific inflow off eastern New Zealand. *Marine Geology* **205**, 9–27. doi: [10.1016/S0025-3227\(04\)00016-7](https://doi.org/10.1016/S0025-3227(04)00016-7).

- Carter L, Carter RM, McCave IN and Gamble J (1996) Regional sediment recycling in the abyssal Southwest Pacific Ocean. *Geology* **24**, 735–8. doi: [10.1130/0091-7613\(1996\)024<0735:RSRITA>2.3.CO;2](https://doi.org/10.1130/0091-7613(1996)024<0735:RSRITA>2.3.CO;2).
- Carter L and McCave IN (1994) Development of sediment drifts approaching an active plate margin under the SW Pacific Deep Western Boundary Current. *Paleoceanography* **9**, 1061–85. doi: [10.1029/94PA01444](https://doi.org/10.1029/94PA01444).
- Carter L and McCave IN (2002) Eastern New Zealand drifts, Miocene–Recent. In *Deep-Water Contourite Systems: Modern Drifts and Ancient Series, Seismic and Sedimentary Characteristics* (eds DAV Stow, CJ Pudsey, JA Howe, J-C Faugères and AR Viana), pp. 385–407. Geological Society of London, Memoirs no. 22. doi: [10.1144/GSL.MEM.2002.022.01.27](https://doi.org/10.1144/GSL.MEM.2002.022.01.27).
- Carter RM, McCave IN, Richter C, Carter L, Aita Y, Buret C, Di Stefano A, Fenner J, Fothergill P, Gradstein F, Hall I, Handwerker D, Harris S, Hayward B, Hu S, Joseph L, Khim BK, Lee Y-D, Millwood L, Rinna J, Smith G, Suzuki A, Weedon G, Wei K-Y, Wilson G and Winkler A (1999) *Proceedings of the Ocean Drilling Program, Initial Reports, vol. 181*. College Station, Texas. doi: [10.2973/odp.proc.ir.181.2000](https://doi.org/10.2973/odp.proc.ir.181.2000).
- Casalbore D (2018) Volcanic islands and seamounts. In *Submarine Geomorphology* (eds A Micallef, S Krastel and A Savini), pp. 333–47. Cham: Springer International Publishing. doi: [10.1007/978-3-319-57852-1\\_17](https://doi.org/10.1007/978-3-319-57852-1_17).
- Chaigneau A, Dominguez N, Eldin G, Vasquez L, Flores R, Grados C and Echevin V (2013) Near-coastal circulation in the Northern Humboldt Current System from shipboard ADCP data. *Journal of Geophysical Research: Oceans* **118**, 5251–66. doi: [10.1002/jgrc.20328](https://doi.org/10.1002/jgrc.20328).
- Chun COJ and Delaney ML (2006) Phosphorus, barium, manganese, and uranium concentrations and geochemistry, Nazca Ridge Site 1237 sediments. In *Proceedings of the Ocean Drilling Project, Scientific Results, vol. 202* (eds R Tiedemann, AC Mix, C Richter and WF Ruddiman), pp. 1–19. College Station, Texas. doi: [10.2973/odp.proc.sr.202.205.2006](https://doi.org/10.2973/odp.proc.sr.202.205.2006).
- Clift PD (2017) A revised budget for Cenozoic sedimentary carbon subduction. *Reviews of Geophysics* **55**, 97–125. doi: [10.1002/2016RG000531](https://doi.org/10.1002/2016RG000531).
- Clift PD, Pecher I, Kukowski N and Hampel A (2003) Tectonic erosion of the Peruvian forearc, Lima Basin, by subduction and Nazca Ridge collision. *Tectonics* **22**, 1023. doi: [10.1029/2002TC001386](https://doi.org/10.1029/2002TC001386).
- Cormier M-H and Sloan H (2018) Abyssal hills and abyssal plains. In *Submarine Geomorphology* (eds A Micallef, S Krastel and A Savini), pp. 389–408. Cham: Springer International Publishing. doi: [10.1007/978-3-319-57852-1\\_20](https://doi.org/10.1007/978-3-319-57852-1_20).
- D'Hondt SL, Jørgensen BB, Miller DJ, Aiello IW, Bekins B, Blake R, Cragg BA, Cypionka H, Dickens GR, Ferdeman T, Ford K, Gettemy GL, Guérin G, Hinrichs K-U, Holm N, House C, Inagaki F, Meister P, Mitterer RM, Naehr T, Niitsuma S, Parkes RJ, Schippers A, Skilbeck CG, Smith DC, Spivack AJ, Teske A and Wiegel J (2003) *Proceedings of the Ocean Drilling Program, Initial Reports, vol. 201*. College Station, Texas. doi: [10.2973/odp.proc.ir.201.2003](https://doi.org/10.2973/odp.proc.ir.201.2003).
- Donda F, Brancolini G, Santis LD and Trincardi F (2003) Seismic facies and sedimentary processes on the continental rise off Wilkes Land (East Antarctica): evidence of bottom current activity. *Deep Sea Research Part II: Topical Studies in Oceanography* **50**, 1509–27. doi: [10.1016/S0967-0645\(03\)00075-4](https://doi.org/10.1016/S0967-0645(03)00075-4).
- Dubois N and Mitchell NC (2012) Large-scale sediment redistribution on the equatorial Pacific seafloor. *Deep Sea Research Part I: Oceanographic Research Papers* **69**, 51–61. doi: [10.1016/j.dsr.2012.07.006](https://doi.org/10.1016/j.dsr.2012.07.006).
- Dutkiewicz A, Müller RD, O'Callaghan S and Jónasson H (2015) Census of seafloor sediments in the world's ocean. *Geology* **43**, 795–8. doi: [10.1130/G36883.1](https://doi.org/10.1130/G36883.1).
- Emery WJ (2019) Water types and water masses. In *Encyclopedia of Ocean Sciences (Third Edition)* (eds JK Cochran, HJ Bokuniewicz and PL Yager), pp. 169–79. Oxford: Academic Press. doi: [10.1016/B978-0-12-409548-9.04426-2](https://doi.org/10.1016/B978-0-12-409548-9.04426-2).
- Emery WJ and Meincke J (1986) Global water masses: summary and review. *Oceanologica Acta* **9**, 383–91.
- Esentia I, Stow D and Smillie Z (2018) Contourite drifts and associated bedforms. In *Submarine Geomorphology* (eds A Micallef, S Krastel and A Savini), pp. 301–31. Cham: Springer International Publishing. doi: [10.1007/978-3-319-57852-1\\_16](https://doi.org/10.1007/978-3-319-57852-1_16).
- Espurt N, Baby P, Brusset S, Roddaz M, Hermoza W, Regard V, Antoine P-O, Salas-Gismondi R and Bolaños R (2007) How does the Nazca Ridge subduction influence the modern Amazonian foreland basin? *Geology* **35**, 515–18. doi: [10.1130/G23237A.1](https://doi.org/10.1130/G23237A.1).
- Faugères J-C, Stow DA, Imbert P and Viana A (1999) Seismic features diagnostic of contourite drifts. *Marine Geology* **162**, 1–38. doi: [10.1016/S0025-3227\(99\)00068-7](https://doi.org/10.1016/S0025-3227(99)00068-7).
- Flood RD and Shor AN (1988) Mud waves in the Argentine Basin and their relationship to regional bottom circulation patterns. *Deep Sea Research Part A. Oceanographic Research Papers* **35**, 943–71. doi: [10.1016/0198-0149\(88\)90070-2](https://doi.org/10.1016/0198-0149(88)90070-2).
- GEBCO Compilation Group 2019 (2019) *The GEBCO\_2019 Grid – A Continuous Terrain Model of the Global Oceans and Land*. Liverpool: British Oceanographic Data Centre, National Oceanography Centre, NERC. doi: [10.5285/836f016a-33be-6ddc-e053-6c86abc0788e](https://doi.org/10.5285/836f016a-33be-6ddc-e053-6c86abc0788e).
- Gomes PO and Viana AR (2002) Contour currents, sediment drifts and abyssal erosion on the northeastern continental margin off Brazil. In *Deep-Water Contourite Systems: Modern Drifts and Ancient Series, Seismic and Sedimentary Characteristics* (eds DAV Stow, CJ Pudsey, JA Howe, J-C Faugères and AR Viana), pp. 239–48. Geological Society of London, Memoirs no. 22. doi: [10.1144/GSL.MEM.2002.022.01.17](https://doi.org/10.1144/GSL.MEM.2002.022.01.17).
- Grove TL, Till CB and Krawczynski MJ (2012) The role of H<sub>2</sub>O in subduction zone magmatism. *Annual Review of Earth and Planetary Sciences* **40**, 413–39. doi: [10.1146/annurev-earth-042711-105310](https://doi.org/10.1146/annurev-earth-042711-105310).
- Gutscher M-A, Olivet J-L, Aslanian D, Eissen J-P and Maury R (1999) The “lost Inca plateau”: cause of flat subduction beneath Peru? *Earth and Planetary Science Letters* **171**, 335–41. doi: [10.1016/S0012-821X\(99\)00153-3](https://doi.org/10.1016/S0012-821X(99)00153-3).
- Hampel A (2002) The migration history of the Nazca Ridge along the Peruvian active margin: a re-evaluation. *Earth and Planetary Science Letters* **203**, 665–79. doi: [10.1016/S0012-821X\(02\)00859-2](https://doi.org/10.1016/S0012-821X(02)00859-2).
- Hampel A, Kukowski N, Bialas J, Huebscher C and Heinbockel R (2004) Ridge subduction at an erosive margin: the collision zone of the Nazca Ridge in southern Peru. *Journal of Geophysical Research: Solid Earth* **109**, B02101. doi: [10.1029/2003JB002593](https://doi.org/10.1029/2003JB002593).
- Harris PT and Macmillan-Lawler M (2018) Origin and geomorphic characteristics of ocean basins. In *Submarine Geomorphology* (eds A Micallef, S Krastel and A Savini), pp. 111–34. Cham: Springer International Publishing. doi: [10.1007/978-3-319-57852-1\\_8](https://doi.org/10.1007/978-3-319-57852-1_8).
- Harris PT, Macmillan-Lawler M, Rupp J and Baker EK (2014) Geomorphology of the oceans. *Marine Geology* **352**, 4–24. doi: [10.1016/j.margeo.2014.01.011](https://doi.org/10.1016/j.margeo.2014.01.011).
- Heezen BC and Hollister C (1964) Deep-sea current evidence from abyssal sediments. *Marine Geology* **1**, 141–74. doi: [10.1016/0025-3227\(64\)90012-X](https://doi.org/10.1016/0025-3227(64)90012-X).
- Hernández-Molina FJ, Llave E and Stow DAV (2008) Chapter 19 continental slope contourites. In *Contourites* (eds M Rebesco and A Camerlenghi), pp. 379–408. Developments in Sedimentology vol. 60. doi: [10.1016/S0070-4571\(08\)10019-X](https://doi.org/10.1016/S0070-4571(08)10019-X).
- Hodel F, Grespan R, de Rafélis M, Dera G, Lezin C, Nardin E, Rouby D, Aretz M, Steinman M, Buatier M, Lacan F, Jeandel C and Chavagnac V (2021) Drake Passage gateway opening and Antarctic Circumpolar Current onset 31 Ma ago: the message of foraminifera and reconsideration of the Neodymium isotope record. *Chemical Geology* **570**, 120171. doi: [10.1016/j.chemgeo.2021.120171](https://doi.org/10.1016/j.chemgeo.2021.120171).
- Horn M and Uenzelmann-Neben G (2015) The Deep Western Boundary Current at the Bounty Trough, east of New Zealand: indications for its activity already before the opening of the Tasmanian Gateway. *Marine Geology* **362**, 60–75. doi: [10.1016/j.margeo.2015.01.011](https://doi.org/10.1016/j.margeo.2015.01.011).
- Johnson GC (2008) Quantifying Antarctic Bottom Water and North Atlantic Deep Water volumes. *Journal of Geophysical Research: Oceans* **113**, C05027. doi: [10.1029/2007JC004477](https://doi.org/10.1029/2007JC004477).
- Juan C, Van Rooij D and De Bruycker W (2018) An assessment of bottom current controlled sedimentation in Pacific Ocean abyssal environments. *Marine Geology* **403**, 20–33. doi: [10.1016/j.margeo.2018.05.001](https://doi.org/10.1016/j.margeo.2018.05.001).
- Kerr BC, Scholl DW and Klemperer SL (2005) Seismic stratigraphy of Detroit Seamount, Hawaiian-Emperor seamount chain: post-hot-spot

- shield-building volcanism and deposition of the Meiji drift. *Geochemistry, Geophysics, Geosystems* **6**, Q07L10. doi: [10.1029/2004GC000705](https://doi.org/10.1029/2004GC000705).
- King DJ and Wade BS** (2017) The extinction of *Chiloguembelina cubensis* in the Pacific Ocean: implications for defining the base of the Chattian (upper Oligocene). *Newsletters on Stratigraphy* **50**, 311–39. doi: [10.1127/nos/2016/0308](https://doi.org/10.1127/nos/2016/0308).
- Koenitz D, White N, McCave IN and Hobbs R** (2008) Internal structure of a contourite drift generated by the Antarctic Circumpolar Current. *Geochemistry, Geophysics, Geosystems* **9**, Q06012. doi: [10.1029/2007GC001799](https://doi.org/10.1029/2007GC001799).
- Kolla V, Eitrem S, Sullivan L, Kosteki JA and Burckle LH** (1980) Current-controlled, abyssal microtopography and sedimentation in Mozambique Basin, southwest Indian Ocean. *Marine Geology* **34**, 171–206. doi: [10.1016/0025-3227\(80\)90071-7](https://doi.org/10.1016/0025-3227(80)90071-7).
- Kukowski N, Hampel A, Hoth S and Bialas J** (2008) Morphotectonic and morphometric analysis of the Nazca plate and the adjacent offshore Peruvian continental slope – implications for submarine landscape evolution. *Marine Geology* **254**, 107–20. doi: [10.1016/j.margeo.2008.05.017](https://doi.org/10.1016/j.margeo.2008.05.017).
- Kukowski N and Oncken O** (2006) Subduction erosion – the “Normal” mode of fore-arc material transfer along the Chilean margin? In *The Andes: Active Subduction Orogeny* (eds O Oncken, G Chong, G Franz, P Giese, H-J Götze, VA Ramos, MR Strecker and P Wigger), pp. 217–36. Berlin, Heidelberg: Springer. doi: [10.1007/978-3-540-48684-8\\_10](https://doi.org/10.1007/978-3-540-48684-8_10).
- Lamb S and Davis P** (2003) Cenozoic climate change as a possible cause for the rise of the Andes. *Nature* **425**, 792–7. doi: [10.1038/nature02049](https://doi.org/10.1038/nature02049).
- Land LA, Paull CK and Spiess FN** (1999) Abyssal erosion and scarp retreat: Deep Tow observations of the Blake Escarpment and Blake Spur. *Marine Geology* **160**, 63–83. doi: [10.1016/S0025-3227\(99\)00012-2](https://doi.org/10.1016/S0025-3227(99)00012-2).
- Lawver LA and Gahagan LM** (1998) Opening of Drake Passage and its impact on Cenozoic ocean. In *Tectonic Boundary Conditions for Climate Reconstructions* (eds TJ Crowley and KC Burke), pp. 212–23. New York: Oxford University Press.
- Lonsdale P** (1976) Abyssal circulation of the southeastern Pacific and some geological implications. *Journal of Geophysical Research (1896–1977)* **81**, 1163–76. doi: [10.1029/JC081i006p01163](https://doi.org/10.1029/JC081i006p01163).
- Lonsdale P and Malfait B** (1974) Abyssal dunes of foraminiferal sand on the Carnegie Ridge. *Geological Society of America Bulletin* **85**, 1697–712. doi: [10.1130/0016-7606\(1974\)85<1697:ADOFSO>2.0.CO;2](https://doi.org/10.1130/0016-7606(1974)85<1697:ADOFSO>2.0.CO;2).
- Lyle M, Gibbs S, Moore TC and Rea DK** (2007) Late Oligocene initiation of the Antarctic Circumpolar Current: evidence from the South Pacific. *Geology* **35**, 691–4. doi: [10.1130/G23806A.1](https://doi.org/10.1130/G23806A.1).
- Magee C, Hunt-Stewart E and Jackson CAL** (2013) Volcano growth mechanisms and the role of sub-volcanic intrusions: insights from 2D seismic reflection data. *Earth and Planetary Science Letters* **373**, 41–53. doi: [10.1016/j.epsl.2013.04.041](https://doi.org/10.1016/j.epsl.2013.04.041).
- Marani M, Argani A, Roveri M and Trincardi F** (1993) Sediment drifts and erosional surfaces in the central Mediterranean: seismic evidence of bottom-current activity. *Sedimentary Geology* **82**, 207–20. doi: [10.1016/0037-0738\(93\)90122-L](https://doi.org/10.1016/0037-0738(93)90122-L).
- Mitchell NC and Huthnance JM** (2013) Geomorphological and geochemical evidence ( $^{230}\text{Th}$  anomalies) for cross-equatorial currents in the central Pacific. *Deep Sea Research Part I: Oceanographic Research Papers* **78**, 24–41. doi: [10.1016/j.dsr.2013.04.003](https://doi.org/10.1016/j.dsr.2013.04.003).
- Mitchum RM, Jr, Vail PR and Sangree JB** (1977) Seismic stratigraphy and global changes of sea level, part 6: stratigraphic interpretation of seismic reflection patterns in depositional sequences. In *Seismic Stratigraphy – Applications to Hydrocarbon Exploration* (ed. CE Payton), pp. 117–33. American Association of Petroleum Geologists Memoir no. 26. doi: [10.1306/M26490C8](https://doi.org/10.1306/M26490C8).
- Mix A** (1997) *Report and Index of Underway Marine Geophysical Data: Genesis Expedition LEG 3 (GENE03RR) R/V Revelle*. La Jolla: Geological Data Center, Scripps Institution of Oceanography.
- Mulder T, Ducassou E, Hanquiez V, Principaud M, Fauquembergue K, Tournadour E, Chabaud L, Reijmer J, Recouvreur A, Gillet H, Borgomano J, Schmitt A and Moal P** (2019) Contour current imprints and contourite drifts in the Bahamian archipelago. *Sedimentology* **66**, 1192–221. doi: [10.1111/sed.12587](https://doi.org/10.1111/sed.12587).
- Müller RD, Sdrolias M, Gaina C and Roest WR** (2008) Age, spreading rates and spreading symmetry of the world’s ocean crust. *Geochemistry, Geophysics, Geosystems* **9**, Q04006. doi: [10.1029/2007GC001743](https://doi.org/10.1029/2007GC001743).
- Nielsen T, Knutz PC and Kuijpers A** (2008) Chapter 16 seismic expression of contourite depositional systems. In *Contourites* (eds M Rebesco and A Camerlenghi), pp. 301–21. Developments in Sedimentology vol. 60. doi: [10.1016/S0070-4571\(08\)10016-4](https://doi.org/10.1016/S0070-4571(08)10016-4).
- Pälike H, Lyle MW, Nishi H, Raffi I, Ridgwell A, Gamage K, Klaus A, Acton G, Anderson L, Backman J, Baldauf J, Beltran C, Bohaty SM, Bown P, Busch W, Channell JET, Chun COJ, Delaney M, Dewangan P, Dunkley Jones T, Edgar KM, Evans H, Fitch P, Foster GL, Gussone N, Hasegawa H, Hathorne EC, Hayashi H, Herrle JO, Holbourn A, Hovan S, Hyeong K, Iijima K, Ito T, Kamikuri S, Kimoto K, Kuroda J, Leon-Rodriguez L, Malinverno A, Moore TC, Jr, Murphy BH, Murphy DP, Nakamura H, Ogane K, Ohneiser C, Richter L, Sluijs A, Takata H, Tian J, Tsujimoto A, Wade BS, Westerhold T, Wilkens R, Williams T, Wilson PA, Yamamoto Y, Yamamoto S, Yamazaki T and Zeebe RE** (2012) A Cenozoic record of the equatorial Pacific carbonate compensation depth. *Nature* **488**, 609–14. doi: [10.1038/nature11360](https://doi.org/10.1038/nature11360).
- Parnell-Turner R, White NJ, McCave IN, Henstock TJ, Murton B and Jones SM** (2015) Architecture of North Atlantic contourite drifts modified by transient circulation of the Icelandic mantle plume. *Geochemistry, Geophysics, Geosystems* **16**, 3414–35. doi: [10.1002/2015GC005947](https://doi.org/10.1002/2015GC005947).
- Pilger RH, Jr** (1981) Plate reconstructions, aseismic ridges, and low-angle subduction beneath the Andes. *Geological Society of America Bulletin* **92**, 448–56. doi: [10.1130/0016-7606\(1981\)92<448:PRARAL>2.0.CO;2](https://doi.org/10.1130/0016-7606(1981)92<448:PRARAL>2.0.CO;2).
- Plank T and Manning CE** (2019) Subducting carbon. *Nature* **574**, 343–52. doi: [10.1038/s41586-019-1643-z](https://doi.org/10.1038/s41586-019-1643-z).
- Planke S, Rasmussen T, Rey SS and Myklebust R** (2005) Seismic characteristics and distribution of volcanic intrusions and hydrothermal vent complexes in the Vøring and Møre basins. In *Petroleum Geology: North-West Europe and Global Perspectives – xxix Proceedings of the 6th Petroleum Geology Conference vol. 6* (eds Doré AG and Vining BA), pp. 833–44. London: Geological Society of London. doi: [10.1144/0060833](https://doi.org/10.1144/0060833).
- Rea DK and Leinen M** (1985) Neogene history of the calcite compensation depth and lysocline in the South Pacific Ocean. *Nature* **316**, 805–7. doi: [10.1038/316805a0](https://doi.org/10.1038/316805a0).
- Rebesco M, Hernández-Molina FJ, Van Rooij D and Wählin A** (2014) Contourites and associated sediments controlled by deep-water circulation processes: state-of-the-art and future considerations. *Marine Geology* **352**, 111–54. doi: [10.1016/j.margeo.2014.03.011](https://doi.org/10.1016/j.margeo.2014.03.011).
- Rebesco M and Stow D** (2001) Seismic expression of contourites and related deposits: a preface. *Marine Geophysical Researches* **22**, 303–8. doi: [10.1023/A:1016316913639](https://doi.org/10.1023/A:1016316913639).
- Reed DL, Meyer AW, Silver EA and Prasetyo H** (1987) Contourite sedimentation in an intraoceanic forearc system: Eastern Sunda Arc, Indonesia. *Marine Geology* **76**, 223–41. doi: [10.1016/0025-3227\(87\)90031-4](https://doi.org/10.1016/0025-3227(87)90031-4).
- Rees BA, Detrick R and Coakley BJ** (1993) Seismic stratigraphy of the Hawaiian flexural moat. *Geological Society of America Bulletin* **105**, 189–205. doi: [10.1130/0016-7606\(1993\)105<0189:Ssothf>2.3.Co;2](https://doi.org/10.1130/0016-7606(1993)105<0189:Ssothf>2.3.Co;2).
- Rosenbaum G, Giles D, Saxon M, Betts PG, Weinberg RF and Duboz C** (2005) Subduction of the Nazca Ridge and the Inca Plateau: insights into the formation of ore deposits in Peru. *Earth and Planetary Science Letters* **239**, 18–32. doi: [10.1016/j.epsl.2005.08.003](https://doi.org/10.1016/j.epsl.2005.08.003).
- Rousse S, Gilder S, Farber D, McNulty B, Patriat P, Torres V and Sempere T** (2003) Paleomagnetic tracking of mountain building in the Peruvian Andes since 10 Ma. *Tectonics* **22**, 1048. doi: [10.1029/2003TC001508](https://doi.org/10.1029/2003TC001508).
- Ryan MC, Helland-Hansen W, Johannessen EP and Steel RJ** (2009) Erosional vs. accretionary shelf margins: the influence of margin type on deepwater sedimentation: an example from the Porcupine Basin, offshore western Ireland. *Basin Research* **21**, 676–703. doi: [10.1111/j.1365-2117.2009.00424.x](https://doi.org/10.1111/j.1365-2117.2009.00424.x).
- Scher HD and Martin EE** (2006) Timing and climatic consequences of the opening of Drake Passage. *Science* **312**, 428–30. doi: [10.1126/science.1120044](https://doi.org/10.1126/science.1120044).
- Scher HD, Whittaker JM, Williams SE, Latimer JC, Kordesch WEC and Delaney ML** (2015) Onset of Antarctic Circumpolar Current 30 million years ago as Tasmanian Gateway aligned with westerlies. *Nature* **523**, 580. doi: [10.1038/nature14598](https://doi.org/10.1038/nature14598).

- Sepulchre P, Sloan LC, Snyder M and Fiechter J** (2009) Impacts of Andean uplift on the Humboldt Current system: a climate model sensitivity study. *Paleoceanography* **24**, PA4215. doi: [10.1029/2008PA001668](https://doi.org/10.1029/2008PA001668).
- Shaffer G, Hormazabal S, Pizarro O and Ramos M** (2004) Circulation and variability in the Chile Basin. *Deep Sea Research Part I: Oceanographic Research Papers* **51**, 1367–86. doi: [10.1016/j.dsr.2004.05.006](https://doi.org/10.1016/j.dsr.2004.05.006).
- Shaffer G, Salinas S, Pizarro O, Vega A and Hormazabal S** (1995) Currents in the deep ocean off Chile (30°S). *Deep Sea Research Part I: Oceanographic Research Papers* **42**, 425–36. doi: [10.1016/0967-0637\(95\)99823-6](https://doi.org/10.1016/0967-0637(95)99823-6).
- Shipboard Scientific Party** (1976) Site 321. In *Initial Reports of the Deep Sea Drilling Project, vol. 34* (eds RS Yeats, SR Hart, JM Ade-Hall, MN Bass, WE Benson, RA Hart, PG Quilty, HM Sachs, MH Salisbury and TL Vallier), pp. 111–53. Washington: U.S. Government Printing Office. doi: [10.2973/dsdp.proc.34.105.1976](https://doi.org/10.2973/dsdp.proc.34.105.1976).
- Shipboard Scientific Party** (1988) Introduction, objectives, and principal results, Leg 112, Peru continental margin. In *Proceedings of the Ocean Drilling Program, Initial Reports, vol. 112* (eds E Suess, R von Huene, K-C Emeis, J Bourgeois, J del C Cruzado Castañeda, P De Wever, G Eglinton, R Garrison, M Greenberg, E Herrera Paz, P Hill, M Ibaraki, M Kastner, AES Kemp, K Kvenvolden, R Langridge, N Lindsley-Griffin, AW Sanchez Fernandez, H-J Schrader, T Thornburg, G Wefer and M Yamano), pp. 5–23. College Station, Texas. doi: [10.2973/odp.proc.ir.112.102.1988](https://doi.org/10.2973/odp.proc.ir.112.102.1988).
- Shipboard Scientific Party** (1992) Introduction. In *Proceedings of the Ocean Drilling Program, Initial Reports, vol. 138* (eds LA Mayer, NG Pisias, TR Janecek, JG Baldauf, SF Bloomer, KA Dadey, K-C Emeis, J Farrell, JA Flores, EM Galimov, TK Hagelberg, P Holler, SA Hovan, M Iwai, AES Kemp, DC Kim, G Klinkhammer, M Leinen, S Levi, MA Levitan, MW Lyle, AK MacKillop, LM Meynadier, AC Mix, TC Moore, Jr, I Raffi, C Ravelo, D Schneider, NJ Shackleton, J-P Valet and E Vincent), pp. 5–12. College Station, Texas. doi: [10.2973/odp.proc.ir.138.101.1992](https://doi.org/10.2973/odp.proc.ir.138.101.1992).
- Shipboard Scientific Party** (1999) Leg 181 summary: Southwest Pacific paleoceanography. In *Proceedings of the Ocean Drilling Program, Initial Reports, vol. 181* (eds RM Carter, IN McCave, C Richter, L Carter, Y Aita, C Buret, A Di Stefano, J Fenner, P Fothergill, F Gradstein, I Hall, D Handwerker, S Harris, B Hayward, S Hu, L Joseph, BK Khim, Y-D Lee, L Millwood, J Rinna, G Smith, A Suzuki, G Weedon, K-Y Wei, G Wilson and A Winkler), pp. 1–80. College Station, Texas. doi: [10.2973/odp.proc.ir.181.101.2000](https://doi.org/10.2973/odp.proc.ir.181.101.2000).
- Shipboard Scientific Party** (2003a) Leg 202 summary. In *Proceedings of the Ocean Drilling Program, Initial Reports, vol. 202* (eds AC Mix, R Tiedemann, P Blum, FF Abrantes, H Benway, I Cacho-Lascorz, M-T Chen, ML Delaney, J-A Flores, L Giosan, AE Holbourn, T Irino, M Iwai, LH Joseph, HF Kleiven, F Lamy, SP Lund, P Martinez, JF McManus, US Ninnemann, NG Pisias, RS Robinson, JS Stoner, A Sturm, MW Wara and W Wei), pp. 1–145. College Station, Texas. doi: [10.2973/odp.proc.ir.202.101.2003](https://doi.org/10.2973/odp.proc.ir.202.101.2003).
- Shipboard Scientific Party** (2003b) Site 1231. In *Proceedings of the Ocean Drilling Program, Initial Reports, vol. 201* (eds SL D'Hondt, BB Jørgensen, DJ Miller, IW Aiello, B Belkins, R Blake, BA Cragg, H Cypionka, GR Dickens, T Ferdelman, K Ford, GL Gettemy, G Guérin, K-U Hinrichs, N Holm, C House, F Inagaki, P Meister, RM Mitterer, T Naehr, S Niitsuma, RJ Parkes, A Schippers, CG Skilbeck, DC Smith, AJ Spivack, A Teske and J Wiegand), pp. 1–64. College Station, Texas. doi: [10.2973/odp.proc.ir.201.112.2003](https://doi.org/10.2973/odp.proc.ir.201.112.2003).
- Southard JB, Young RA and Hollister CD** (1971) Experimental erosion of calcareous ooze. *Journal of Geophysical Research (1896–1977)* **76**, 5903–9. doi: [10.1029/JC076i024p05903](https://doi.org/10.1029/JC076i024p05903).
- Stein CA and Stein S** (1992) A model for the global variation in oceanic depth and heat flow with lithospheric age. *Nature* **359**, 123–9. doi: [10.1038/359123a0](https://doi.org/10.1038/359123a0).
- Stow DAV, Faugères J-C, Gonthier E, Cremer M, Llave E, Hernández-Molina FJ, Somoza L and Diaz-Del-Rio V** (2002) Faro-Albufeira drift complex, northern Gulf of Cadiz. In *Deep-Water Contourite Systems: Modern Drifts and Ancient Series, Seismic and Sedimentary Characteristics* (eds DAV Stow, CJ Pudsey, JA Howe, J-C Faugères and AR Viana), pp. 137–54. Geological Society of London, Memoirs no. 22. doi: [10.1144/gsl.Mem.2002.022.01.11](https://doi.org/10.1144/gsl.Mem.2002.022.01.11).
- Stow D, Smillie Z, Pan J and Esentia I** (2019) Deep-sea contourites: sediments and cycles. In *Encyclopedia of Ocean Sciences (Third Edition)* (eds JK Cochran, HJ Bokuniewicz and PL Yager), pp. 111–20. Oxford: Academic Press. doi: [10.1016/B978-0-12-409548-9.10879-6](https://doi.org/10.1016/B978-0-12-409548-9.10879-6).
- Talley LD** (2013) Closure of the global overturning circulation through the Indian, Pacific, and Southern Oceans: schematics and transports. *Oceanography* **26**, 80–97. doi: [10.5670/oceanog.2013.07](https://doi.org/10.5670/oceanog.2013.07).
- Tiedemann R and Mix A** (2007) Leg 202 synthesis: southeast Pacific paleoceanography. In *Proceedings of the Ocean Drilling Program, Scientific Results, vol. 202* (eds R Tiedemann, AC Mix, C Richter and WF Ruddiman), pp. 1–56. College Station, Texas. doi: [10.2973/odp.proc.sr.202.201.2007](https://doi.org/10.2973/odp.proc.sr.202.201.2007).
- Thran AC, Dutkiewicz A, Spence P and Müller RD** (2018) Controls on the global distribution of contourite drifts: insights from an eddy-resolving ocean model. *Earth and Planetary Science Letters* **489**, 228–40. doi: [10.1016/j.epsl.2018.02.044](https://doi.org/10.1016/j.epsl.2018.02.044).
- Tsuchiya M and Talley LD** (1998) A Pacific hydrographic section at 88°W: water-property distribution. *Journal of Geophysical Research* **103**, 12899–918. doi: [10.1029/97JC03415](https://doi.org/10.1029/97JC03415).
- Vail PR, Todd RG and Sangree JB** (1977) Seismic stratigraphy and global changes of sea level, part 5: chronostratigraphy significance of seismic relations. In *Seismic Stratigraphy – Applications to Hydrocarbon Exploration* (ed. CE Payton), pp. 99–116. American Association of Petroleum Geologists Memoir no. 26. doi: [10.1306/M26490C8](https://doi.org/10.1306/M26490C8).
- Velde B** (1996) Compaction trends of clay-rich deep sea sediments. *Marine Geology* **133**, 193–201. doi: [10.1016/0025-3227\(96\)00020-5](https://doi.org/10.1016/0025-3227(96)00020-5).
- von Huene R, Pecher IA and Gutscher M-A** (1996) Development of the accretionary prism along Peru and material flux after subduction of Nazca Ridge. *Tectonics* **15**, 19–33. doi: [10.1029/95TC02618](https://doi.org/10.1029/95TC02618).
- von Humboldt A** (1816) *Voyage aux régions équinoxiales du Nouveau Continent fait en 1799, 1800, 1801, 1802, 1803 et 1804, par Al. De Humboldt et A. Bonpland, rédigé par Alexandre de Humboldt, avec un atlas géographique et physique, Tome Second*. Paris: Librairie Greque-Latine-Allemande, 382 pp.
- Wold CN** (1994) Cenozoic sediment accumulation on drifts in the northern North Atlantic. *Paleoceanography* **9**, 917–41. doi: [10.1029/94PA01438](https://doi.org/10.1029/94PA01438).
- Wolfe CJ, McNutt MK and Detrick RS** (1994) The Marquesas archipelagic apron: seismic stratigraphy and implications for volcano growth, mass wasting, and crustal underplating. *Journal of Geophysical Research: Solid Earth* **99**, 13591–608. doi: [10.1029/94JB00686](https://doi.org/10.1029/94JB00686).
- Wright NM, Seton M, Williams SE and Müller RD** (2016) The Late Cretaceous to recent tectonic history of the Pacific Ocean basin. *Earth-Science Reviews* **154**, 138–73. doi: [10.1016/j.earscirev.2015.11.015](https://doi.org/10.1016/j.earscirev.2015.11.015).
- Yu X, Stow D, Smillie Z, Esentia I, Brackenridge R, Xie X, Bankole S, Ducassou E and Llave E** (2020) Contourite porosity, grain size and reservoir characteristics. *Marine and Petroleum Geology* **117**, 104392. doi: [10.1016/j.marpetgeo.2020.104392](https://doi.org/10.1016/j.marpetgeo.2020.104392).
- Zachos J, Pagani M, Sloan L, Thomas E and Billups K** (2001) Trends, rhythms, and aberrations in global climate 65 Ma to Present. *Science* **292**, 686–93. doi: [10.1126/science.1059412](https://doi.org/10.1126/science.1059412).